A Review of Electromagnetic Compatibility/Interference Measurement Methodologies

MARK T. MA, FELLOW, IEEE, MOTOHISA KANDA, SENIOR MEMBER, IEEE, MYRON L. CRAWFORD, SENIOR MEMBER, IEEE, AND EZRA B. LARSEN, MEMBER, IEEE

Invited Paper

This paper presents a review summary of radiated emission and susceptibility measurement methodologies currently used for assessing the electromagnetic compatibility/interference (EMC/EMI) characteristics of electronic devices and systems. In particular, measurement methods using open sites, transverse electromagnetic (TEM) cells, reverberating chambers, and anechoic chambers are discussed, in light of their technical justifications and bases, their strengths and limitations, and interpretation of the measured results.

I. Introduction

Electromagnetic compatibility/interference (EMC/EMI) may not be household words yet, but their effects are apparent in almost every place because of the prolific use of electronics and digital circuits in products such as television sets, personal computers, microwave ovens, and automobiles. Over the years, several terms have been used to connote the electromagnetic environment such as radio frequency interference (RFI), radio noise, electromagnetic pollution, EMC and EMI. The *IEEE Dictionary* defines EMC and EMI as follows [1]:

EMC: The capability of electronic equipment or systems to be operated in the intended operational electromagnetic environment at designed levels of efficiency.

EMI: Impairment of a wanted electromagnetic signal by an electromagnetic disturbance.

One of the first recorded cases of EMI was documented in 1927 by the Federal Aviation Agency [2]. They observed an aircraft altimeter was giving faulty readings and the problem was caused by interference generated by the ignition system of the aircraft. The first EMC military standard was published in 1945, entitled "Interference Measurements, Radio, Methods of 150 kc to 20 Mc (for components and complete assemblies)" [3].

Some electronic equipment such as transmitters are designed to supply radio-frequency (RF) power at selected frequencies to antennas, from which the signal is radiated intentionally. Signals which may also radiate other than at the intended frequencies are undesirable and called spurious emissions, a form of EMI. Other electronic equipment such as computers are designed to function as nonradiators. Ideally, a computer will perform its tasks and all signals generated within the system will be contained and not be radiated; however, some of these internal signals are not totally contained and are radiated as EMI.

The process of establishing electromagnetic compatibility (EMC) with electronic equipment usually requires two steps. The first step is to make measurements to determine if any undesired signals being radiated from the equipment (radiated EMI) and/or appearing on the power lines, control lines, or data lines of the equipment (conducted EMI) exceed limits set forth by the using agency.

The second step is to expose the electronic equipment to selected levels of electromagnetic (EM) fields at various frequencies to determine if the equipment can perform satisfactorily in its intended operational environment. Exposing the equipment to EM fields of various strengths is referred to as susceptibility or immunity testing.

The limits or requirements set forth for EMC testing are usually established by regulatory agencies such as:

1) Federal Communications Commission (FCC), USA,
2) Department of Defense (DoD), EMC Military Standards,
3) Interdepartmental Special Committee on Radio Interference (IRAC), USA,
4) National Center for Devices and Radiological Health (NCDRH), USA,
5) Verboard Deutscher Elektrotechniker (VDE), West Germany,
6) other foreign agencies.

Manuscript received May 11, 1984; revised December 10, 1984.

The authors are with the Electromagnetic Fields Division, United States Department of Commerce, National Bureau of Standards, Boulder, CO 80303, USA.

In addition to the specifications by these regulatory agencies, there are a number of voluntary EMI standards available for use. These standards are usually published by professional organizations that utilize the expertise of many who donate their time and effort in the preparation of documents. A few examples of these organizations are:

1) American National Standards Committee C63 on Radio-Electrical Coordination,
2) American National Standards Committee C95 on RF Radiation Levels for Personal Safety,
3) Institute of Electrical and Electronics Engineers, Inc. (IEEE), EMC Society Standards Committee,
4) Society of Automotive Engineers (SAE),
5) Electronic Industries Association (EIA) G46 Committee on EMC,
6) Radio Technical Commission for Aeronautics (RTCA),
7) International Special Committee on Radio Interference (CISPR),
8) International Standards Organization (ISO).

There are numerous measurement methods available for making EMC/EMI tests depending on the following considerations:

1) size of the test equipment,
2) frequency range,
3) test limits,
4) types of field to be measured (electric or magnetic),
5) polarization of the field,
6) electrical characteristics of the test signal (frequency or time domain).

Because each method has limitations of one kind or another, no one method is ideal for all tests. Certain regulatory standards such as MIL-STD 462 [4] or FCC part 15 [5] do specify a particular method.

The purpose of this paper is to review some of these radiated EMC/EMI measurement methods, in which the National Bureau of Standards (NBS) at Boulder, CO, has made significant contributions during the past two decades. The technical justifications and bases for these methods, and interpretations of the measured results are emphasized, as well as their strengths and limitations. The methods to be covered are:

1) open sites,
2) transverse electromagnetic (TEM) cells,
3) revrberating chambers,
4) anechoic chambers.

Some other related methods and features which are variations of the above, such as the underground low-Q enclosures and parallel plates, are briefly commented on. In addition, since a small probe antenna plays an important role in EMC/EMI measurements, including some of the measurement methods reviewed in this paper, a section on various probe systems developed at NBS is also provided.

II. Open-Site Measurements

Traditionally, open-site measurements provide a straightforward approach to evaluating the EMI performance of the electronic equipment involved. One important parameter to be determined by this method is the site attenuation or insertion loss between a source and a receiver. More precisely, it is defined as the ratio of the input power to the source antenna (or the voltage at the source signal generator) to the power induced at the load impedance connected to the receiving antenna (or the voltage appearing across the load) [6]–[9]. To facilitate the evaluation of this parameter, a pair of transmitting and receiving antennas is usually set up above the ground, with or without a metal ground plane, as shown in Fig. 1. The parameter is then

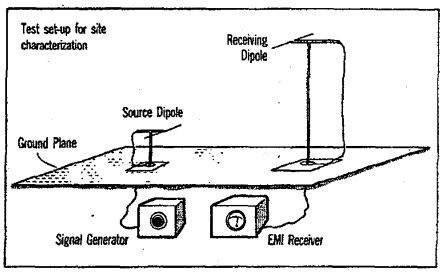

Fig. 1. A typical outdoor open-site test setup.

determined as a function of frequency, separation distance between the antennas, and their respective heights above the ground. Sometimes, the relative insertion loss, defined as the power indicated by the receiver at an initial separation distance between the antennas compared with that at different separation distances, is evaluated instead [10]. The quality of measurements made using an earth ground plane depends on the ground constants. For more reliable results, a metal ground plane or screen of finite size is normally recommended. Difference between the measured site of attenuation and the theoretical result based on an ideal site (infinitely large in size and perfectly conducting) will then serve as an indication of site imperfections.

With this facility, it is convenient to perform both radiated emission and susceptibility tests for large systems over a wide frequency range. There are, of course, obvious disadvantages associated with this method of measurement such as requiring a sizable measurement site and that the surrounding area be free of metallic objects. Also, there is a lack of isolation between the experimental setup and the external EM environment. This lack of isolation results in subjecting the facility to unfavorable weather conditions, limiting emission tests by the ambient noise level, and limiting susceptibility tests by FCC restrictions.

Frequent occurrences of significant disagreement between the measured results of site attenuation or insertion loss and those obtained by the conventional, simple, analytical computation creates considerable concern within the EMC community. The disagreement becomes more pronounced and often exceeds the tolerance permitted by the regulatory authority when the antennas are in close proximity (within the near-field range) of each other. This occurs, for example, at frequencies below about 50 MHz for a 3-m separation distance recommended by the International Electrotechnical Commission [11], the CISPR [12], and the FCC [8] for some measurements. The disagreement between the theoretical and measured results occurs mainly because the conventional computation is based on the use of a free-space antenna impedance and a far-field condition, and because the effects of a ground plane and the mutual coupling between the two antennas are ignored [8],

[11]–[13]. Another reason for disagreement is that the experimental results are typically obtained by computation with the measured receiver voltage and an assumed value of antenna factor supplied by the manufacturer, which is dependent upon a given site attenuation [14]. Here the antenna factor is defined as the electric-field strength appearing at the receiving antenna divided by the voltage developed at the 50-Ω receiver. Thus the unknown electric field is determined by multiplying the antenna factor by the measured receiver pickup voltage. However, the antenna factor is, almost without exception, calibrated or computed under the far-field and free-space conditions. For an example, in accordance with the definition given above, the antenna factor (AF) for a linear dipole in free space may be written as

$$\mathrm{AF} = \frac{1}{\ell_e} \cdot \frac{|50 + Z_{\mathrm{in}}|}{50}$$

$$= \frac{\pi}{\lambda} \cot(kh/2) \cdot \frac{|50 + Z_{\mathrm{in}}|}{50} \qquad \mathrm{m}^{-1} \qquad (1)$$

where λ is the operating wavelength in meters, k is the wavenumber ($2\pi/\lambda$), h is the half physical length of the dipole in meters, ℓ_e and Z_{in} are, respectively, the effective length in meters and the open-circuit input impedance in ohms of the dipole. A sinusoidal current distribution on a very thin dipole has been assumed [15].

For a practical resonant dipole, $Z_{\mathrm{in}} = 70\ \Omega$, and $kh = 0.47\pi$ (depending on the length-to-radius ratio of the dipole and frequency), the antenna factor may be approximately expressed as

$$\mathrm{AF} = 0.02762f \qquad \mathrm{m}^{-1}$$

or

$$\mathrm{AF} = 20\log f - 31.18 \qquad \mathrm{dB} \qquad (2)$$

where f is the operating frequency in megahertz.

The presence of a ground plane changes the antenna impedance. An example showing variations of the input impedance (both resistive and reactive parts) of a horizontal half-wave dipole ($kh = \pi/2$) as a function of the antenna height above a perfectly conducting plane of infinite extent is given in Fig. 2 [16]. This curve also assumes a thin wire and a sinusoidal current distribution. Thus when the half-wave horizontal dipole is placed 0.25 λ above a perfect ground as the measuring antenna, its input impedance becomes approximately $Z_{\mathrm{in}} = 85.6 + j72.4\ \Omega$. The antenna factor will then be modified to

$$\mathrm{AF} = 20\log f - 29.84 \qquad \mathrm{dB} \qquad (3)$$

resulting in a shift of greater than 1 dB from the free-space value.

Furthermore, if the measuring antenna is relatively close to the source antenna, the mutual coupling [9], [14], near fields, and surface-wave excitations [10], [17], [18] (depending on frequency, polarization, and ground condition) may also be important factors to consider. As a consequence, the antenna response could be quite different from that obtained in free space. The use of a free-space antenna factor without paying due attention to the condition under which radiated EMI measurements are performed may, therefore, cause significant errors in results.

Recently, a more rigorous method of computing the 3-m site attenuation for two identical horizontal half-wave dipoles was proposed [19]. This method using a formulation of coupled integral equations for the antenna currents includes the ground and mutual coupling effects. It also takes into consideration possible impedance mismatches between the antenna and measuring equipment, and the influence of the antenna wire size. The method requires, however, numerical computations by the method of moments [20], and does not treat the case of vertical dipoles.

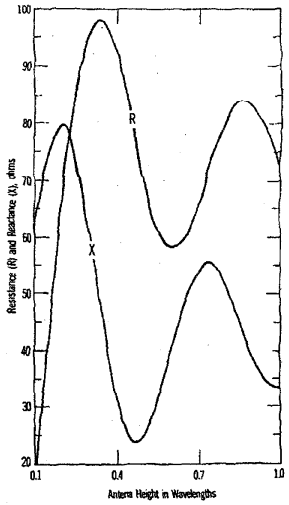

Fig. 2. Variations in input impedance of a half-wave dipole above a perfect ground plane.

For vertical polarized dipoles, theoretical results of site attenuation obtained recently by including the mutual coupling effects have also shown better agreement with the measured data than before [14]. A critique on this method has already been received [21]. A method different from the established methods [22], [23] for calibrating the antenna factor under a practical operating environment has also been proposed [24]. Once the site attenuation and the related antenna factor are properly modified by including the practical factors discussed above, the accuracy of determining an unknown electric-field strength by the open-site measurement method should be satisfactory.

III. Transverse Electromagnetic (TEM) Cells

One of the main limitations inherent in all EMC/EMI susceptibility tests is the requirement of an antenna to represent the source. Typical antennas are bandwidth limited, and do not have linear phase response versus frequency. Hence, they are useful primarily for frequency-domain measurements, and their applications to transient, impulsive EMI testing and evaluation are very limited. In addition, for accurate measurements, the separation distance between the antenna and equipment under test (EUT) should be sufficiently large to ensure far-field conditions. This is not always possible, especially in confined chambers or enclosures. Quite often, the requirement of sensitivity and high-level testing field dictate the need for near-field measurements. Such requirements introduce another problem related to field uniformity over the test volume occupied by the EUT and interaction effects. Some of these difficulties may be eliminated or minimized by using TEM

cells, because they themselves serve as the transducer and thus eliminate the use of antennas.

The TEM cell was designed based on the concept of an expanded transmission line operated in a TEM mode. As shown in Fig. 3, it consists of a section of rectangular coaxial transmission line (RCTL) with tapered sections at

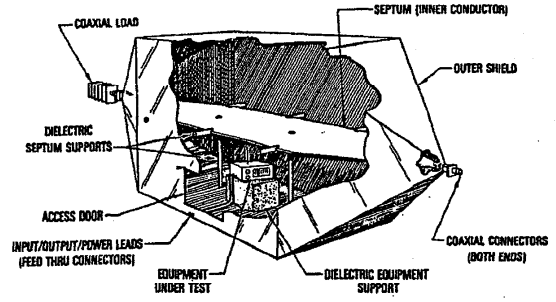

Fig. 3. An NBS TEM cell.

both ends. The taper is used as a transition to match the RCTL to standard 50-Ω coaxial-cable connectors at the two ports of the cell. The taper sections should be gradual and long enough to minimize perturbation of the TEM wave as it passes from one section to the other. It is generally recommended that this length be at least one half of the cell's width. One of the two ports is usually terminated with a 50-Ω load, while the other port is connected to either a source or a receiver, depending on whether the cell is used for radiated susceptibility or emission testing. The TEM cell provides a shielded environment without introducing multiple reflections experienced with conventional shielded enclosure [25]. Hence, external EM signals will not affect the measurement of low-level radiated emission from the EUT, or high-level test field generated inside a cell for performing susceptibility tests will not interfere with external electronic systems.

To support a TEM mode, the cell is necessarily a two-conductor system with the region between the inner and outer conductors (either upper or lower chamber) used as the test zone. The cross section of a TEM cell is depicted in Fig. 4. Although the center septum (inner conductor) is normally designed to be midway between the top and bottom outer conductors, its position can be modified to have a vertical offset to allow a larger test zone provided by one of the

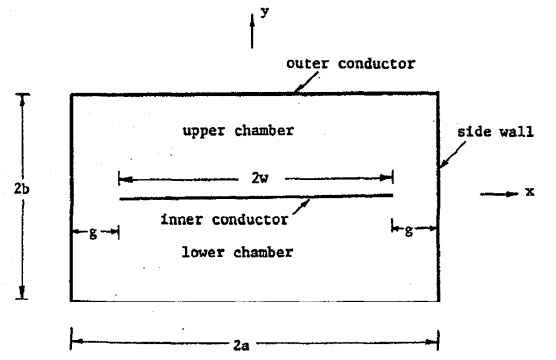

Fig. 4. Cross section of a TEM cell.

chambers [26], [27]. We limit our discussions in this paper only to the symmetrically located inner conductor, however.

TEM cells offer several advantages in performing EMC/EMI measurements of electrically small equipment and devices. They are portable, simple to build [28], useful for broad-band swept-frequency measurements, and capable of providing test field strengths from a few microvolts per meter to a few hundred volts per meter. The cost to build a TEM cell is much lower than that for conventional facilities such as anechoic chambers and shielded enclosures. The TEM field generated between the inner and outer conductors simulates very closely a planar far field in free space, and has constant amplitude and linear phase characteristics [29].

The application of TEM cells has limitations too. The usable frequency range is from dc to an upper limit determined by the appearance of the lowest high-order mode [26], [29], [30]. The volume available for testing purpose is inversely proportional to this upper frequency limit. In addition, since the EUT is placed at the center of the test zone, its size should be small relative to the test volume in order that the field structure associated with the ideal TEM mode existing in an empty cell will not be significantly perturbed.

The most important aspect for a TEM cell user to recognize is that the results obtained from the measurements made inside a cell have to be interpreted correctly in terms of the corresponding free-space results, because the characteristics of an EUT inside a TEM cell are different from those in other environments such as free space [31]. This interpretation is especially crucial if a meaningful comparison with other measurement methods is attempted.

Before presenting the details of using a TEM cell to make radiated susceptibility and emission tests, we summarize some basic TEM cell properties as follows.

Impedance Consideration: The characteristic impedance, Z_0, of an RCTL may be expressed in terms of the distributed capacitance per unit length of the transmission line, C_0, by [26], [31]:

$$Z_0 = \eta_0 \epsilon_0 / C_0 \tag{4}$$

where $\eta_0 = 120\pi$ is the free-space intrinsic impedance in ohms, and

$$\epsilon_0 = \frac{1}{36\pi}(10)^{-9}$$

is the air permittivity in farads per meter.

Determination of C_0 may be formulated through elliptic integrals and then computed numerically [26], [31]. If the aspect ratio is small, i.e., $b/a \leq 1$, then an approximate expression for C_0/ϵ_0 may be obtained [31]

$$C_0/\epsilon_0 \cong 4\left[\frac{w}{b} + \frac{2}{\pi}\ln\left(1 + \coth\frac{\pi g}{2b}\right)\right] - \frac{\Delta C}{\epsilon_0} \tag{5}$$

where the cell parameters a, b, g, and w, all in meters, are indicated in Fig. 4. In this form, it is easy to identify the first term, $4w/b$, as the plate capacitance between the center septum and the horizontal walls (top and bottom outer conductors), the second term involving the gap parameter g as the fringing capacitance between the edge of the septum and the vertical sidewalls, and the third term $\Delta C/\epsilon_0$ as a correction needed to account for the interaction between

the two edges. However, under the practical condition, $w/b \geq 1/2, \Delta C$ is negligible.

If a characteristic impedance value of, say, 50 Ω is desirable, we then require $C_0/\epsilon_0 = 7.54$. A number of possible TEM cells may be designed, based on (5), to meet this requirement.

Higher Order Mode Consideration: As mentioned before, the upper frequency limit for a TEM cell is determined by the appearance of the lowest higher order mode. In addition, the associated resonances occuring in the cell may also limit the frequency range. The cutoff wavelengths of the first few higher order gap-perturbed modes in the cell are presented in Fig. 5 [26], [30], [31], [33], [34]. From these

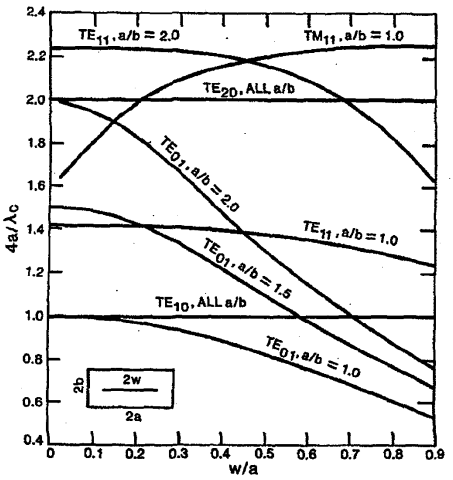

Fig. 5. Cutoff wavelength of the first higher order gap-perturbed mode in a TEM cell.

data, one can easily estimate the approximate cutoff frequencies. Note that this estimation is based totally on the cross section of the cell whose length is assumed to be infinitely long. In reality, the cell is finite and the two ends are tapered; hence, the actual measured cutoff frequencies are somewhat different from the theoretical estimation. The resonance frequency, f_{res}, associated with a mode of cutoff frequency, f_c, can be found from the following expression:

$$f_{res} = \left[f_c^2 + (c/2d)^2 \right]^{1/2} \tag{6}$$

where $c = 3(10)^8$ m/s is the speed of light, and d (in meters) is the resonance length. Again, because of the tapered sections at the two ends, the resonance length is not well defined. As a first approximation, an average "overall cell length" is usually taken as the resonance length [30].

It is important to note that a) the influence of the first-order TE modes does not become significant until approaching a resonant frequency, and b) if the septum of the cell is centered symmetrically, the odd-order TE modes are not excited in the empty cell (these modes may exist when an EUT is placed in the cell). Thus the upper useful frequency can exceed the multimode cutoff frequency of the first higher order mode, but should be less than this mode's associated resonant frequency. For example, the cutoff and resonance frequencies for a cell with $a = b =$ 1 m, $w/a = 0.8$ (or $g/a = 0.2$), and $d = 4$ m are approximately 43 and 66 MHz. Such a cell should be useful at frequencies up to approximately 60 MHz.

Efforts have been made to extend the use of TEM cells to frequencies above cutoff by installing RF absorbers inside the cell [35]. While this effort helps to lower the Q factor of the cell and suppress the multimoding effects, it also has some effect on the fundamental TEM mode. Thus care must be exercised when considering the placement of absorbing materials inside a TEM cell.

Field Distribution: An analytical expression for the electric field inside an empty TEM cell over the cross section shown in Fig. 4, when operated in a TEM mode, is also available in terms of Jacobian elliptical functions [26], [32]. Numerical results for the electric field in a typical symmetric cell are presented in Fig. 6. The results have been normalized with respect to V/b, which represents the elec-

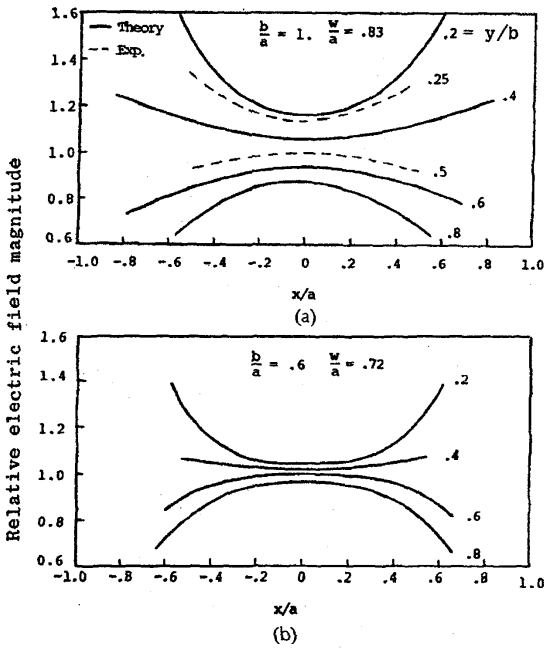

Fig. 6. Normalized magnitude of the electric field of the TEM mode inside an RCTL. (a) $b/a = 1$, $w/a = 0.83$. (b) $b/a = 0.6$, $w/a = 0.72$.

tric field at the center of the test zone ($x = 0, y = b/2$) where

$$V = (P_n Z_0)^{1/2} \tag{7}$$

is the voltage in volts between the inner and outer conductors, P_n the net power in watts flowing through the cell, and Z_0 the characteristic impedance in ohms given in (4). Field distribution for certain higher order modes, while not the major concern of TEM cell users, may be found elsewhere [26], [36].

Radiated Susceptibility Test: As mentioned above, the TEM cell was developed as an alternative to the conventional shielded enclosure for EMC/EMI testing of electronic equipment. It is useful especially at frequencies below a

few hundred megahertz. The main purpose of radiated susceptibility testing is to determine if and how EM energy is coupled into the EUT to cause possible degradation to equipment performance. Thus a criterion of measuring the degradation is normally established first by the user. This criterion may be in the form of video or audio indicators, or by other means when the EMI coupling exceeds a predetermined threshold. The following measurement procedure in terms of steps is suggested as a systematic approach for making a radiated susceptibility evaluation [36], [37].

The first step is to place the EUT in a TEM cell centered in the lower half space below the septum (or upper half). The first position (position A) as shown in Fig. 7 is near the floor

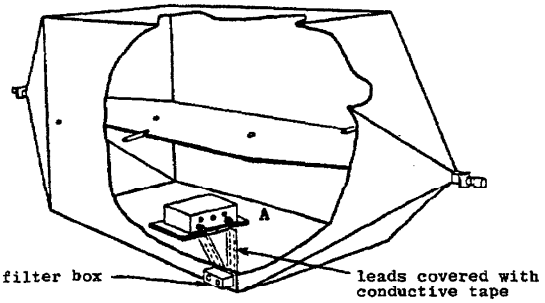

Fig. 7. Placement of EUT near floor of TEM cell for minimum exposure of leads to the field.

but insulated from the floor with approximately 2 cm of foam dielectric. Plastic foams with a dielectric constant of 1.04 to 1.08 are readily available, are almost invisible electrically, and make good supporting material. If grounding of the equipment case is desired, the EUT would then be placed on the floor. This position (position A) is used to minimize exposure of the EUT's input/output leads to the test field. Another common EUT position (herein called position B) for testing is midway between the septum and the floor. Again, the EUT is supported on a low dielectric foam material. This position increases the exposure of leads to the test field. A comparison of the test results to be taken later for both positions A and B may give some indication of how energy is coupled into the EUT. After placing the EUT in positions A and B, we may reorient the EUT as desired, relative to the cell's field polarization. Typically, the first orientation is with the EUT lying flat as in normal use. Care must be taken to record the placement location and how this is done so that it can be repeated if necessary. It may be helpful to mark the bottom of the cell with a uniform array of scribe marks to assist in determining placement locations precisely.

The second step is to access the EUT as required for operation and performance monitoring. The EUT input/output and ac power cables should be as nearly the same as in its anticipated use. Cables should be the same length if possible, be terminated into their equivalent operational impedances so as to simulate the EUT in its operational configuration, and be carefully routed inside the cell to minimize field perturbation. Dielectric guides or holders may be installed in the cell to assure repeatability of the placement location of the cables. These may be placed on the floor to allow the cables to be covered with conductive tape (minimum exposure) and/or on dielectric standoffs to provide coupling of the test field to the leads. If required, a portion of the EUT's leads (wiring harness) may be carefully bundled together in a coil and covered with conductive tape on the floor of the cell. When the leads are bundled together, it may be helpful to twist the input/output/monitor leads as separate conductor pairs or use shielded cables to minimize cross coupling between them. It may also be necessary to space the windings in the coil to avoid introducing resonances associated with the coil inductance and distributed capacitance. If braided RF shielding is used, it should be in electrical contact with the cell floor, and not in contact with the case of the EUT unless a common ground between the EUT and cell is required. Grounding the two together will influence the results of the susceptibility measurements. The input and output leads, after being connected to the appropriate feedthroughs for accessing and operating the EUT, should also be filtered to prevent RF leakage into the cell, otherwise the shielding integrity of the measurement system will suffer. Care must be exercised in selecting these filters so they do not significantly affect the measured results. The monitor leads used for sensing and telemetering the performance of the EUT may require special high-resistance lines made of carbon-impregnated plastic or fiber optic lines to prevent perturbation of, or interaction with, the test environment. DC signals or signals with frequency components below 1 kHz may be monitored via the high-resistance lines. RF signals should be monitored via fiber optic lines.

If the monitor signal is at a frequency or frequencies sufficiently different from the susceptibility test frequency or frequencies, metallic leads may be used with appropriate filtering (high-pass, low-pass, band-pass, etc.) at the bulkhead. Such leads, however, will cause some perturbation of the test field, thus their placement location must be carefully defined for future reference. Note that a separate, shielded filter compartment should be provided on the outside of the cell for housing the filters, as shown in Fig. 7.

The third step is to connect up the measurement system as shown in Figs. 8 or 9 for the frequency range 10 to 500 MHz. At frequencies below 10 MHz, the dual directional coupler and power meters are replaced by a voltage monitor Tee and RF voltmeter. The system shown in Fig. 8 is for swept-frequency testing, while that in Fig. 9 is for automated discrete-frequency testing. The testing operation in Fig. 9 is under computer control thus allowing the test field level in the cell to be carefully controlled and progressively increased at selected frequencies while monotoring the EUT performance. If degradation occurs as determined from a pre-established threshold and evidenced by a sensor, the computer can respond by limiting the test field level to prevent damage to the EUT. The computer also prints out the susceptibility information according to software instruction and format.

The fourth step is to initialize the measurement system by recording the EUT monitor response and test-field measurement instrumentation with the RF source turned off. This includes zeroing the appropriate instrumentation. The RF source is then turned on at the test frequency, modulation rate, test waveform, etc., and its output level is increased gradually until the maximum required test level is reached or the EUT response monitors indicate vulnerability. Care must be exercised to insure that sufficient time is

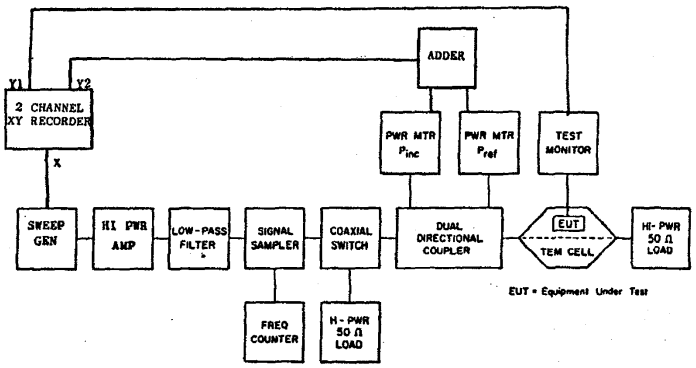

Fig. 8. Block diagram of systems for susceptibility testing of equipment, 10 to 500 MHz.

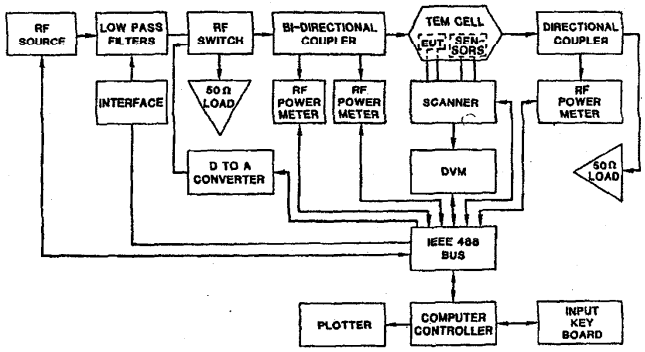

Fig. 9. Block diagram of automated TEM cell susceptibility mesurement system.

spent at each frequency and field level to allow the EUT to respond. The EUT's susceptibility profile is then determined for each test position and orientation. It may be necessary to test all three orthogonal orientations of the EUT inside the cell. This is required if all surfaces of the EUT to be tested are polarization matched to the TEM field of the cell.

If the test frequency is below 10 MHz, the electric field level in volts per meter generated inside the cell is determined by the RF voltmeter reading, V_{RF} in volts, in accordance with V_{RF}/b, where b is the separation in meters between the septum and floor. When the test frequency is 10 MHz or above, where the electric length of the cell is significant, the electric-field level is determined by V/b, where V is given in (7) and the net power may be determined by

$$P_n = C_f P_i - C_r P_r \quad \text{W} \tag{8}$$

with C_f and C_r as the respective forward and reverse coupling ratios of the calibrated bidirectional coupler, and P_i and P_r as the indicated incident and reflected coupler sidearm power readings in watts.

Note that the size of the EUT should be small relative to the test volume inside the cell. When the EUT is not small, it will effectively short out a significant part of the vertical separation resulting in an increase in the field level. In such a case, an effective separation may have to be determined, depending on the EUT height, in order to estimate the actual field level. Details for determining an effective separation distance may be found elsewhere [38].

If the objective of the measurement program is simply to reduce the vulnerability of the EUT to EMI without the additional requirement of determining worst case susceptibility as a function of absolute exposure field level, one EUT orientation with input/output lead configuration may be tested in one particular operational mode under a preselected susceptibility test-field waveform and level. Similar tests may then be duplicated at the same test position with the same lead configuration and test-field waveform and level, after the corrective measures such as providing additional shielding, etc., are made to the EUT. These testing results are then compared to determine the degree of improvement.

Sometimes, it is desirable to monitor the field distribution inside the cell using small calibrated electric and/or magnetic probes, while an EUT is in position. If this is the case, one must be careful in interpreting the monitoring results, because the results are a combination of the incident TEM field launched inside the cell and the scattered fields from the EUT and its leads in the near-field range. The field so monitored can be quite different from the test field, leading to potentially erroneous conclusions. Whenever possible, it is preferable to mount the field monitoring probes in the opposite chamber in the mirror image location of the EUT.

Radiated Emission Test: Electronic equipment not designed as a radiator has unintentional leakage sources which may be considered electrically small. As such, the leakage currents on the exterior surfaces of the electronic equipment, treated here as an EUT, can be modeled as

equivalent electric and magnetic short dipole sources [39]–[41]. These dipole sources may then be combined vectorially to form a composite equivalent source consisting of three orthogonal electric and three orthogonal magnetic dipole moments as represented in Fig. 10, each having an amplitude and a phase.

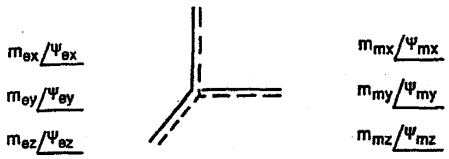

Fig. 10. An unknown electrically small source is considered to be made of equivalent three orthogonal electric and three orthogonal magnetic dipoles.

When an unknown source object (EUT) is placed at the center of a TEM cell, its emission couples into the fundamental TEM mode and propagates toward the two ports of the cell. With a hybrid junction inserted into a loop connecting the cell output as shown in Fig. 11, we are able to measure the sum and difference powers and the relative

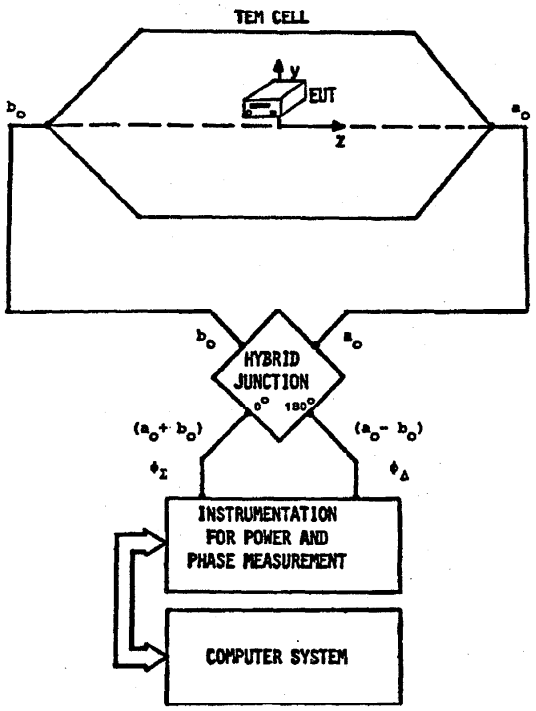

Fig. 11. Emission testing measurement systems.

phase between the sum and difference outputs. This way of measuring the relative phase is very advantageous because it avoids the complication of having to establish an absolute phase reference physically connected to the EUT. Systematic measurements of the powers and relative phases at six different EUT orientations are sufficient to determine the amplitudes and phases of the unknown equivalent component dipole moments as depicted in Fig. 10, from which the corresponding detailed radiation pattern and total power radiated by the unknown source in free space can then be computed [39].

For the purpose of describing the source (EUT) position and related experimental procedures, it is necessary to establish a coordinate system (x, y, z) for the TEM cell with the origin at the geometric center of the inner conductor. The unknown source EUT may be placed at $(0, y_0, 0)$. We assign another coordinate system (x', y', z') with respect to the center of the EUT, as shown in Fig. 12.

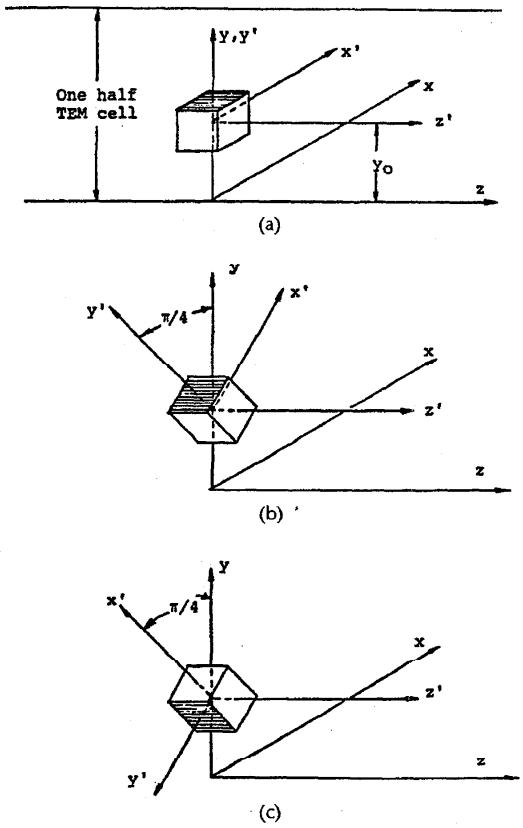

Fig. 12. Two EUT orientations in the TEM cell.

Initially, we align x–x', y–y', and z–z' as shown in Fig. 12(a). The first measurement orientation is obtained by rotating the EUT counterclockwise by an angle of $\pi/4$ about the z'-axis so that its position relative to the TEM cell is shown in Fig. 12(b). We measure the sum and difference powers in watts and the relative phase in degrees between the sum and difference outputs, and designate them, respectively, as P_{s1}, P_{d1}, and ϕ_1. We then rotate the EUT by an additional $\pi/2$, also counterclockwise about the z'-axis as displayed in Fig. 12(c) to the second measurement orientation. We measure the sum power, difference power, and the relative phase between them as P_{s2}, P_{d2}, and ϕ_2.

We next align the coordinate frames such that $x = y'$, $y = z'$, and $z = x'$. Then we rotate the EUT counterclockwise by an angle of $\pi/4$ about the x'-axis serving as the third measurement orientation, take the sum power P_{s3}, difference power P_{d3}, and the relative phase between the

sum and difference outputs ϕ_3. Rotating the EUT counterclockwise by another $\pi/2$ about the x-axis and taking the same sequence of measurements yield P_{s4}, P_{d4}, and ϕ_4.

Finally, we align the coordinate frames in accordance with $x = z'$, $y = x'$, and $z = y'$, rotate the EUT in a similar manner about the y'-axis, and measure P_{s5}, P_{d5}, ϕ_5; P_{s6}, P_{d6}, and ϕ_6.

After collecting the measured sum and difference powers and applying the Lorentz reciprocity theorem, we obtain the following [41]:

$$m_{ex}^2 = (P_{s1} + P_{s2} - P_{s3} - P_{s4} + P_{s5} + P_{s6})/(2q^2) \quad (9)$$

$$m_{ey}^2 = (P_{s1} + P_{s2} + P_{s3} + P_{s4} - P_{s5} - P_{s6})/(2q^2) \quad (10)$$

$$m_{ez}^2 = (-P_{s1} - P_{s2} + P_{s3} + P_{s4} + P_{s5} + P_{s6})/(2q^2) \quad (11)$$

$$m_{mx}^2 = (P_{d1} + P_{d2} - P_{d3} - P_{d4} + P_{d5} + P_{d6})/(2k^2q^2) \quad (12)$$

$$m_{my}^2 = (P_{d1} + P_{d2} + P_{d3} + P_{d4} - P_{d5} - P_{d6})/(2k^2q^2) \quad (13)$$

$$m_{mz}^2 = (-P_{d1} - P_{d2} + P_{d3} + P_{d4} + P_{d5} + P_{d6})/(2k^2q^2) \quad (14)$$

$$m_{ex}m_{ey}\cos\theta_{e1} = (P_{s1} - P_{s2})/(2q^2) \quad (15)$$

$$m_{ey}m_{ez}\cos\theta_{e2} = (P_{s3} - P_{s4})/(2q^2) \quad (16)$$

$$m_{ez}m_{ex}\cos\theta_{e3} = (P_{s5} - P_{s6})/(2q^2) \quad (17)$$

$$m_{mx}m_{my}\cos\theta_{m1} = (P_{d2} - P_{d1})/(2k^2q^2) \quad (18)$$

$$m_{my}m_{mz}\cos\theta_{m2} = (P_{d4} - P_{d3})/(2k^2q^2) \quad (19)$$

$$m_{mz}m_{mx}\cos\theta_{m3} = (P_{d6} - P_{d5})/(2k^2q^2) \quad (20)$$

where

$$\theta_{e1} \equiv \psi_{ex} - \psi_{ey} \qquad \theta_{e2} \equiv \psi_{ey} - \phi_{ez} \qquad \theta_{e3} \equiv \psi_{ez} - \psi_{ex}$$
$$\theta_{m1} \equiv \psi_{mx} - \psi_{my} \qquad \theta_{m2} \equiv \psi_{my} - \phi_{mz} \qquad \theta_{m3} \equiv \psi_{mz} - \psi_{mx} \quad (21)$$

and q is the normalized amplitude of the vertical electric field which would exist at the cell of an empty TEM cell when it is operated in a receiving mode and is excited by an input power of 1 W at one end and terminated at the other end with a matched load. Thus $q = (50)^{1/2}/b$ in $\Omega^{1/2}/m$, which is determined by the height of the cell.

In obtaining (9) through (20), we have assumed that the frequency of the unknown interference source (EUT) to be detected by the spectrum analyzer included in the measurement instrumentation as shown in Fig. 11 is such that it allows only propagation of the dominant mode inside the cell. The size of the interference source to be tested must be small relative to the test volume of the cell. This is required to minimize the potential perturbation to the field distribution inside the cell, as was cautioned before. Under the above assumptions, we see from (9)–(11) that the amplitudes, m_{ei}, $i = x, y, z$, of the unknown component electric dipole moments in ampere-meters are obtainable by the sum powers only, and from (12)–(14) that the amplitudes, m_{mi}, of the unknown component magnetic dipole moments in ampere-square meters are obtainable by the difference powers only.

Once m_{ei} and m_{mi} are determined, they can be used to compute the total power radiated in free space by the same source as

$$P_T = \frac{40\pi^2}{\lambda^2}\left\{ m_{ex}^2 + m_{ey}^2 + m_{ez}^2 + k^2\left(m_{mx}^2 + m_{my}^2 + m_{mz}^2\right)\right\} \quad \text{W.} \quad (22)$$

Note that if one is interested only in determining the total power radiated by the source, which may be the case in practice, all we need to extract are m_{ei}^2 and m_{mi}^2 based on the measured powers.

The corresponding far-field radiation pattern in free space depends, however, also on the relative phases among the component dipole moments of the same and mixed kinds. The former (same kind) can be extracted by (15)–(20) with certain constraining conditions, while the latter (mixed kind), $\psi_{ei} - \psi_{mj}$, $i, j = x, y, z$ but $i \neq j$, is much involved with the component dipole moments determined in (9)–(14) and the measured relative phases ϕ_i, $i = 1, 2, \cdots, 6$, between the sum and difference outputs. This is the reason that these relative phases are also measured and recorded. Detailed procedures of extracting $\psi_{ei} - \psi_{mj}$ may be found elsewhere [41].

Note, however, that if one knows beforehand that the unknown interference source may be characterized by one kind of dipole moment only (either electric or magnetic), the relative phase measurement will not be required [41]. In addition, if the source is believed to be made of electric dipole moments only, then the sum power measurements will suffice to determine the radiation characteristics of the source. Similarly, the difference power measurements will be the dominant ones if the source is essentially magnetic dipoles.

Naturally, when the measured powers and phases are not contaminated by background noise or other inaccuracies, the source parameters so extracted and the radiation characteristics so computed are accurate and proven to be unique [41]. In the practical world, however, the experimental data are always degraded somewhat by background noise, equipment limitations, and the reading accuracy. These measurement imperfections will cause uncertainties in the deduced results. A report giving necessary mathematical derivations for, and performing the analysis of, these uncertainties is available [42].

The method outlined above has been successfully tested by a simulated example and two practical examples, one with a known small spherical dipole representing the electric type [39], [41], and the other with a known small loop antenna representing the magnetic type [43]. The deduced radiation characteristics such as the strength of dipole moment and the total power radiated by the spherical dipole in free space agree very well with the measured results obtained by other means [44].

Before leaving this section, we note that a conventional shielding room may be converted into a TEM cell by installing a flat plate inside the room [45]. Another important option of TEM cells is the parallel-plate or stripline facilities [46]–[49]. The general measurement guideline for these alternative forms is the same as that for TEM cells, except that the fringe field from the parallel plate must be confined to avoid possible damage to or interaction with nearby equipment.

IV. Reverberating Chambers

The limitation on operating frequency for TEM cells as described in Section III could be a drawback for certain applications. Furthermore, since the polarization of the field generated inside a TEM cell is fixed, the radiated emission and susceptibility tests for an EUT using TEM cells requires physical rotations (or different orientations) as discussed. This requirement of EUT rotation could be another inconvenient aspect.

A relatively new EMC/EMI measurement technique, which does not require EUT rotations, is to utilize reverberating chambers to generate an average uniformly homogeneous and isotropic field within a local region inside a metal enclosure [50]–[58]. The polarization of this homogeneous and isotropic field is randomly varying. It is precisely because of this special property that the physical rotation of test objects can be avoided. The homogeneous and isotropic field is achieved by rotating an irregularly shaped mode stirrer or tuner either continuously or in steps [56]. Naturally, the associated boundary conditions are changing with respect to time so that the possible eigenmodes existing simultaneously inside a given shielded metal chamber (cavity) are perturbed accordingly.

Two analytical approaches for treating this type of EM field problem and for providing basic knowledge for design purposes are possible. One involves the direct solution of Maxwell's equations with time-varying boundary conditions. A formal solution using this direct approach is rather difficult to obtain. In the other approach, suitable linear combinations of basic eigenmodes of the unperturbed cavity (without mode stirrer or tuner) with time-dependent expansion coefficients are taken to represent the field and to satisfy approximately the boundary condition on the surface of the rotating-mode stirrer or tuner [56]. The main advantage of this latter approach is that the unperturbed eigenfrequencies and eigenmodes are much easier to calculate, and the problem can be reduced to a more familiar one under special conditions. A necessary condition for the validity of this method is, however, that the total number of eigenmodes which can exist inside a chamber be large for a specified frequency and chamber size. Thus the measurement technique using reverberating chambers is good for very high frequency application, and may serve as a powerful supplementary tool to TEM cells. Typical frequencies of operation are from a few hundred megahertz to 20 GHz or above.

The reverberating chamber is also capable of providing a very efficient conversion of source power to high-intensity fields inside a shielded enclosure for performing EMC/EMI tests of large size of equipment and whole systems. The limiting factors are that users may not feel confident to interpret the measurement results taken inside the chamber and to correlate to actual operating conditions, and that polarization properties are not preserved for characterizing an EUT.

Some Design Considerations

As expected, the total possible number of modes, $N(f)$, inside an unperturbed, lossless, rectangular chamber of dimensions ($a \times b \times d$) is increasing in steps with frequency. A smooth approximation to $N(f)$ has been formulated [56], [57]

$$N_s(f) = \frac{8\pi}{3} abd \frac{f^3}{c^3} - (a + b + d)\frac{f}{c} + \frac{1}{2} \qquad (23)$$

where abd in cubic meters represents the chamber volume, f the operating frequency in hertz, and c the speed of wave propagation in the chamber medium (usually air) in meters per second.

Note that the first term in (23) is identical to Weyl's formula [56] derived originally for the same problem by a different approach, and is proportional to the chamber volume and the third power of frequency. The second term may be recognized as the edge term, which is proportional to the sum of the linear dimensions of the chamber and modifies Weyl's result, especially in the lower frequency range. The inner surface area of the chamber, $2(ab + bd + da)$, is not involved in (23). An example is given in Fig. 13 showing $N(f)$ as Curve 1, $N_s(f)$ as Curve 2, and Weyl's formula as Curve 3 for the NBS chamber. Note that the dimensions of the NBS chamber, 2.74 m × 3.05 m × 4.57 m, are all unequal. Designs of chambers having two or three sides equal but with the same volume will increase mode degeneracy, thus decreasing the total number of distinct modes with respect to a given operating frequency. Under this condition, wider steps in Curve 1 than those shown in Fig. 13 will be observed, even though the smooth approximation (Curve 2) remains almost unchanged.

While the total number of eigenmodes inside an unperturbed chamber is an important design criterion, another equally important factor to consider is the mode density function, dN/df, which represents the change in the number of modes in a given frequency interval. Of course, the exact shape of dN/df involves impulse functions as it is the derivative of step functions. An alternative quantity for exhibiting this property is to examine

$$\Delta N = \int_{\Delta f} \frac{dN}{df}\, df \qquad (24)$$

which represents the increase or decrease in mode number within a frequency interval of Δf.

Results of ΔN when $\Delta f = 1$ MHz are presented in Fig. 14 for the NBS chamber. Clearly, the uniformity of mode distribution in the frequency interval of 1 MHz is good. Indeed, mode distribution uniformity was the main motivation for the unequal dimensions of the NBS chamber. It is not difficult to see that the mode distribution would not be as uniform for those chambers of the same volume but with two or three sides equal. The general design criteria for a reverberating chamber are then to make the volume as large as possible and the ratio of squares of linear dimensions as nonrational as possible.

A third design criterion, namely, the quality factor, may be considered to characterize a reverberating chamber when it is made of lossy material. Since there are so many modes existing in an unperturbed chamber with each mode carrying its own Q-value [56], [57], [59], it is not trivial to define a quality factor for the chamber as a whole. One method of defining a composite quality factor for an unloaded cham-

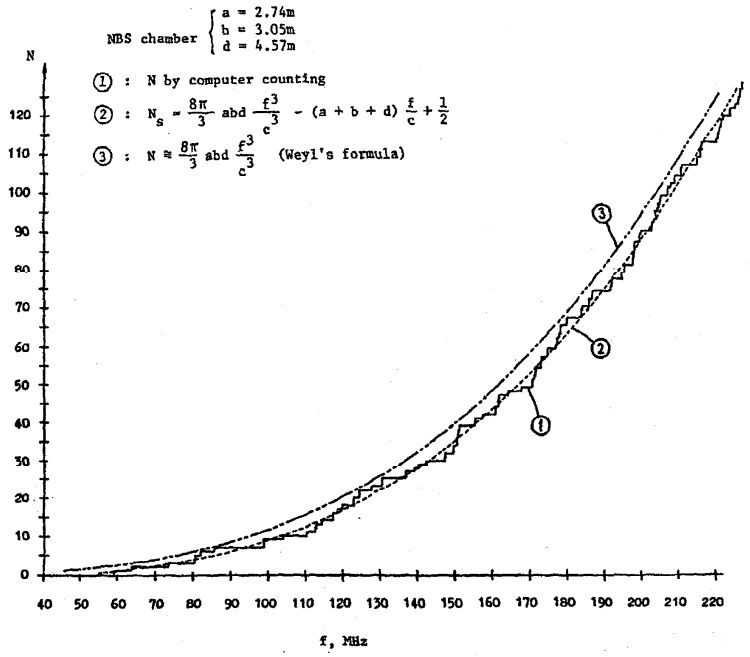

Fig. 13. Total number of modes as a function of operating frequency for the NBS chamber.

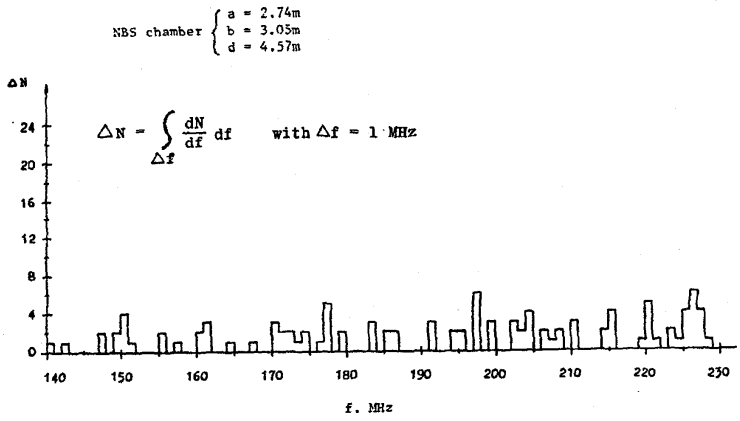

Fig. 14. An illustration of mode density (NBS chamber).

ber (without an EUT in it) within a specified frequency range gives the following simple approximate result [56]:

$$\tilde{Q} = \frac{3}{2}\left(\frac{V}{S\delta_s}\right)\frac{1}{1 + \frac{3\pi}{8k}\left(\frac{1}{a} + \frac{1}{b} + \frac{1}{d}\right)} \qquad (25)$$

where V denotes the chamber volume (abd) in cubic meters, and δ_s the skin depth in meters of the material of the chamber.

The physical meaning of (25) may be interpreted by comparing it with the individual Q-values of all the modes in the form of cumulative distribution. Since $V/(S\delta_s)$ is a common factor whether the composite quality factor defined above or the quality factor for individual modes is considered, it is more convenient to present the results in terms of $1/Q$-values normalized with respect to $S\delta_s/V$. Thus the variable used herein is

$$\alpha = \frac{1}{Q}(V/S\delta_s). \qquad (26)$$

Examples of the cumulative distribution of α for the NBS chamber are given, respectively, in Figs. 15–17 for three different frequency bands. For the frequency band of 180 to 200 MHz in Fig. 15, the total number of modes existing in this band of 20 MHz is 69, with each mode having its own Q-value. The probability of having a high upper bound value of $\alpha \leqslant 0.80$ (or a lower bound for Q) is almost 100 percent, and that for a low value of $\alpha \leqslant 0.48$ (or a high value for Q) is only about 10 percent. This implies that almost all of the 69 modes in this particular frequency band have $\alpha \leqslant 0.80$. The arithmetic mean of 0.623 and the standard deviation of 0.090 are also indicated in the figure. The

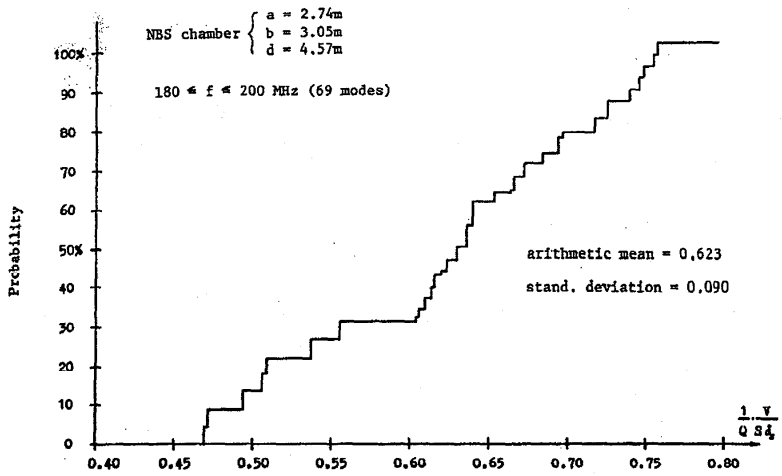

Fig. 15. Cumulative distribution curve of the normalized $1/Q$-values in the 180- to 200-MHz frequency band for the NBS chamber.

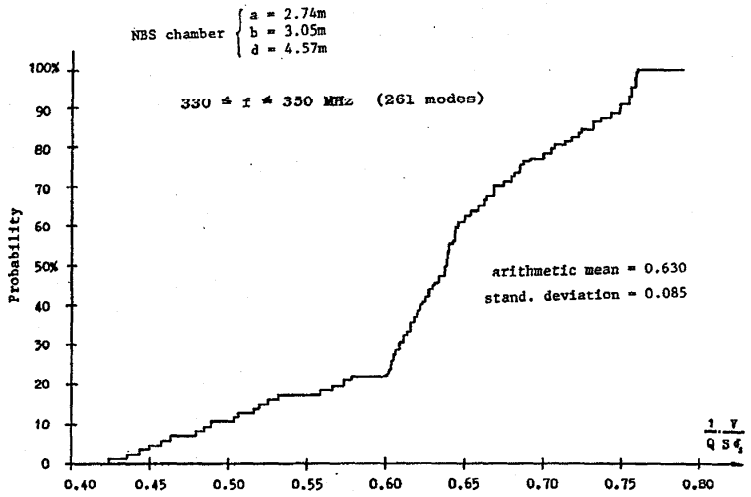

Fig. 16. Cumulative distribution curve of the normalized $1/Q$-values in the 330- to the 350-MHz frequency band for the NBS chamber.

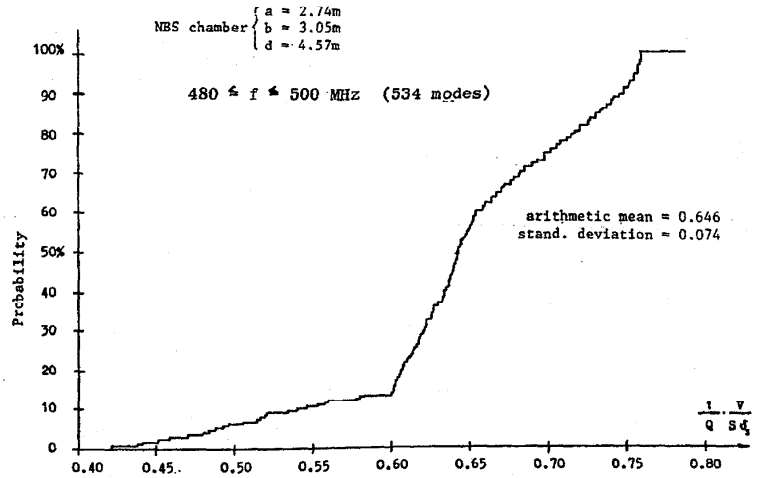

Fig. 17. Cumulative distribution curve of the normalized $1/Q$-values in the 480- to 500-MHz frequency band in the NBS chamber.

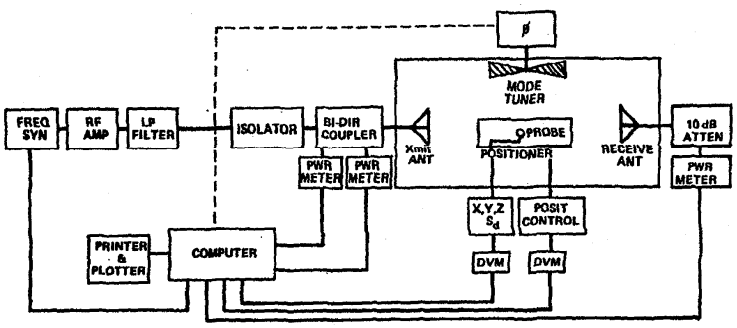

Fig. 18. Block diagram of NBS modified-mode-tuned enclosure system for EMC measurements.

probability of having $\alpha \leqslant 0.623$ (arithmetic mean) is, of course, 50 percent, meaning that at least one half of the 69 modes have $\alpha \leqslant 0.623$.

For the case presented in Fig. 16, where the frequency band is from 330 to 350 MHz, also of a bandwidth of 20 MHz, there are 261 modes, an increase in number of modes relative to that in Fig. 15. This is because of higher frequency. A similar interpretation of the α-values (or Q-values) carried by these modes in terms of probability applies. Note that there are now a small number of modes (low probability) carrying a value of α as low as 0.43 (high Q). The arithmetic mean and standard deviation are, respectively, 0.630 (higher than the corresponding value in Fig. 15) and 0.085 (lower than the corresponding value in Fig. 15). A higher value of arithmetic mean implies that one half or more of the 261 modes carry a higher value of α (lower Q) compared to the frequency band considered in Fig. 15. A decrease in standard deviation reveals that a greater number of modes have α-value closer to the arithmetic mean.

If we consider a still higher frequency band 480 to 500 MHz such as that illustrated in Fig. 17, 534 possible modes will exist in the same bandwidth of 20 MHz. The arithmetic mean increases further to 0.646 while the standard deviation decreases further to 0.074, indicating that a greater number of modes will have still higher α-values near the arithmetic mean. This general tendency, increasing in arithmetic mean and decreasing in standard deviation with increased frequency, yields a limiting mean of $\alpha \leqslant 0.667$ with a 50-percent probability, which also agrees precisely with the limiting value for composite $\tilde{\alpha}$ derived from (25) and (26).

Thus even though there are a large number of possible modes existing in a specified operating frequency band for a reverberating chamber, with each mode carrying its own value of α or Q, the probability that $\alpha \leqslant 0.667$ (or $Q \geqslant 1.5\,V/S\delta_s$) is 50 percent. This implies that one half of the modes have α-values less than 0.667. Preliminary estimation of a quality factor to characterize the reverberating chamber as a whole, based on the simple expression of $\tilde{Q}$ in (25), for the purpose of predicting the field strength level to be generated in the test zone is indeed very useful. The composite quality factor so estimated is considered as the upper bound value because it does not take into account losses other than that due to wall conductivity.

Since compromises between low conductor losses (high Q) and broad modal coverage (low Q) are almost always necessary in the practical design of reverberating chamber, the results for ΔN in (24) and $\tilde{Q}$ in (25) will be found convenient and helpful.

Recent Measurement Results

The basic measurement system used at NBS is shown in Fig. 18. The test field is established by means of one or more RF sources feeding one or more transmitting antennas placed inside the chamber. We use here the log-periodic antenna (0.2 to 1.0 GHz), corrugated horn (1.0 to 4.0 GHz), or double ridged circular horn (4.0 to 18.0 GHz) as the transmitting antenna. Modes excited inside the chamber by the transmitting antenna are then tuned or stirred by rotating one or more field-perturbing devices referred to as "paddlewheel tuner." The tuners are typically electrically large metal blades or irregularly shaped structures that are mounted on the enclosure walls or ceiling driven by electrical motors. The reason for using the irregular shape is to help scatter the field more evenly in all directions. Fig. 19 shows the NBS tuner. The field generated at the test zone is then measured by a calibrated probe as a function of

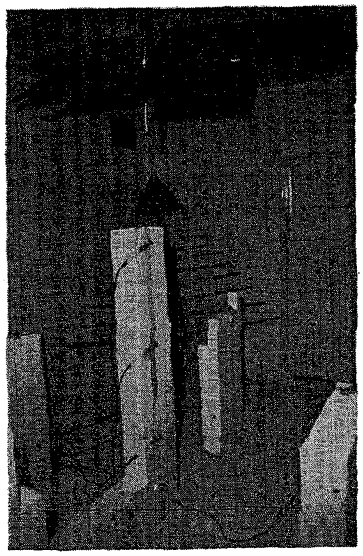

Fig. 19. Photograph of tuner inside NBS reverberating chamber.

frequency and tuner position. Note that there is another receiving antenna placed inside the chamber to measure the maximum and minimum received powers (see Fig. 18). The long-wire antenna (0.2 to 1.0 GHz), corrugated horn (1.0 to 4.0 GHz), or double ridged circular horn (4.0 to 18.0 GHz) is employed as this receiving antenna. The measured data of these received powers are useful for assessing the effectiveness of the tuner, the relative uniformity of the field, and the quality factor of the chamber.

In the mode-stirred case [50], [55], the tuner rotates continuously, thus changing the chamber's boundary conditions, the voltage standing-wave ratio (VSWR) of the transmitting antenna, the net input power to the chamber, and the field polarization and strength. The resultant field is then recorded by detectors with sampling rates much faster than the tuner's rotating speed, and statistically processed. In the mode-tuned case [57], [60], the tuner position is stepped at discrete intervals. Measurements of the net power delivered to the transmitting antenna, power received by the reference antenna, and perhaps also the monitor response of the EUT being tested are taken for each tuner position and frequency. This mode of operation makes possible corrections for the variations in field strength due to changes in the VSWR. An example of the transmitting antenna VSWR variation in the NBS chamber is presented in Fig. 20, giving the maximum, average, and minimum VSWRs as a function of frequency, obtained by

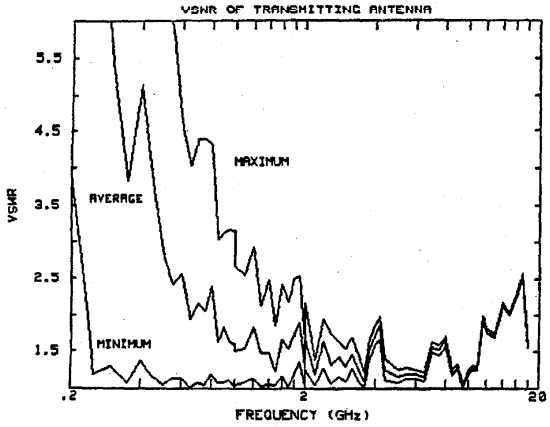

Fig. 20. Variations in VSWR of transmitting antennas placed inside the NBS reverberating chamber. Log-periodic: 0.2–1.0 GHz, corrugated horn: 1.0–4.0 GHz, double rigid circular horn: 4.0–18.0 GHz.

rotating the tuner through a complete revolution with 200 steps (1.8° increments). Note the large variation at the lower frequency end. Failure to correct for this change could result in errors in determining the test field level [61]. At higher frequencies above approximately 2 GHz, variations in VSWR become much more reasonable.

To evaluate the tuner's effectiveness, the ratio of maximum to minimum received powers for a complete revolution at 200 steps is given in Fig. 21 as a function of frequency, showing an average of 30 dB. The net input power to the transmitting antenna has been maintained constant for this measurement. If the tuner were not as effective, the maximum to minimum received power ratio

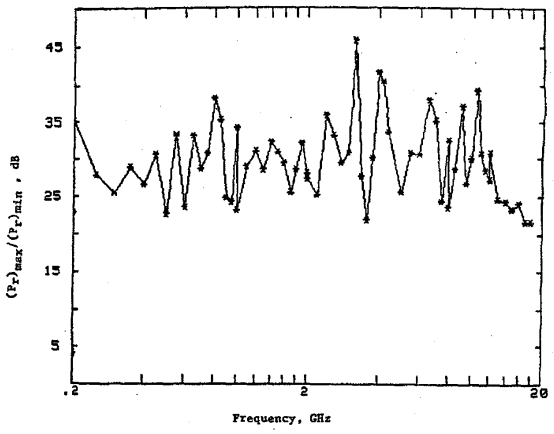

Fig. 21. Maximum to minimum received power ratio as a function of frequency for the NBS chamber and tuner.

would be very low. This fact can be verified by using a much smaller size of tuner with a rather regular shape.

Another important feature characterizing the chamber is the measured difference between the net input power to the transmitting antenna and the power available at the reference antenna terminals. This difference represents the chamber loss, which may be used to estimate the actual mean quality factor of the chamber. This information, of course, is important for considering the power requirement and broad modal coverage. The loss characteristics for the NBS chamber, both the average and minimum losses after rotating the tuner by one complete revolution at 200 steps, are shown in Fig. 22. The smooth solid curves represent

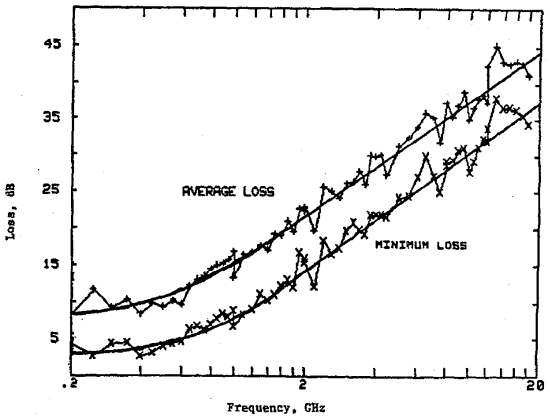

Fig. 22. Loss characteristics for the NBS chamber (empty) with the smooth solid curve representing estimated fits from the measured data.

estimated fits from the measured data. Based on the measured minimum loss data, the actual mean chamber quality factor may be estimated by [51]

$$Q' = 16\pi^2 \frac{V}{\lambda^3} \frac{P_r}{P_t} \tag{27}$$

where P_r is the minimum power available at the reference antenna terminals, P_t is the net power delivered to the transmitting antenna in the same unit as that of P_r, V is the

chamber volume in cubic meters, and λ is the operating wavelength in meters.

The result of (27) is plotted in Fig. 23 as curve (*a*). For comparison purposes, the composite quality factor $\tilde{Q}$ as computed by (25), is also shown in the same figure as curve (*b*). The ratio of $\tilde{Q}/Q'$ is presented in Fig. 24, showing that Q' approaches closer to $\tilde{Q}$ for higher frequencies where more modes are available and the field strength inside the chamber is relatively more uniform.

The maximum and average electric-field strengths generated inside the chamber, as adjusted to 1-W net input power, are presented in Fig. 25 as a function of frequency. The field strengths were measured using an electric-field probe (1-cm dipole) placed at the center of the test zone, with 200 tuner positions. The probe was rotated through three orthogonal orientations aligned with the chamber axes. The magnitude of the total electric field was taken as the square root of the sum of the squared values of the three components. The probe response was calibrated in a planar-field environment at frequencies up to 2.4 GHz. The field strengths at frequencies above 2.4 GHz were also determined by using the same probe response.

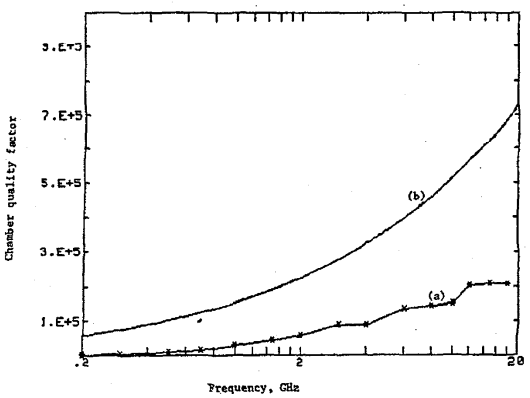

Fig. 23. Quality factor of the NBS chamber: (*a*)—experimental mean Q' obtained from (27) based on measured received power, (*b*)—theoretical composite $\tilde{Q}$ as computed from (25).

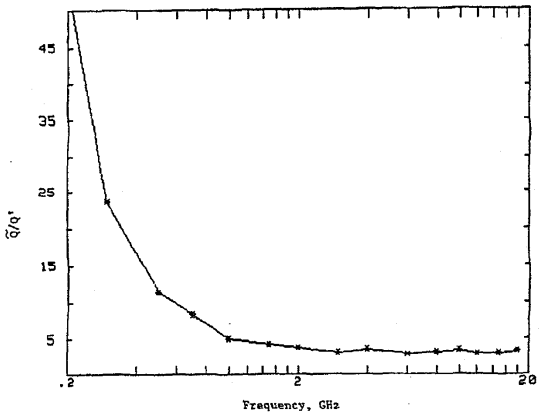

Fig. 24. Ratio of theoretical composite $\tilde{Q}$ to experimental mean Q'.

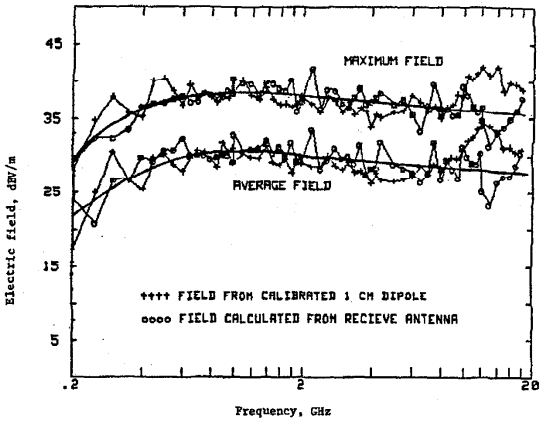

Fig. 25. Maximum and average electric-field strengths generated inside the NBS chamber (empty, mode-tuned).

An increase in field strength at approximately 15 GHz as shown in Fig. 25 is believed due to the probe resonant characteristic rather than due to the chamber. It can be corrected if necessary, by recalibrating the probe at 15 GHz. Also included in Fig. 25 are the field strengths calculated from the power P_r received by the reference antenna in accordance with the following:

$$E_c = \frac{4\pi}{\lambda}(30P_r)^{1/2} \quad \text{V/m.} \tag{28}$$

The above expression was derived based on the assumption of far-field environment. Obviously, such condition does not exist inside a multimode chamber. The expression has been used frequently within the EMC community even though it has received only marginal justifications [50]. The results presented in Fig. 25, however, demonstrate good agreement between the direct measurements and that derived from (28). To increase further our own confidence, we also independently measure the maximum, average, and minimum magnetic fields with a magnetic-field probe (a loop antenna of 1-cm diameter) in a similar manner. The corresponding ratios of the electric field to the magnetic field may be loosely referred to as wave impedances, which vary widely as expected with frequencies. However, the average wave impedance at frequencies above 200 MHz (the lower frequency limit recommended for our chamber) is approximately 120 π. This serves as an additional check to the validity of (28). Thus it appears that (28) can be used as a preliminary means to determine the level of the test field.

It is important to note that the reference antenna type is not significant, except that it is desirable to have its impedance reasonably matched to the power detector especially for high frequencies when more modes are available in the chamber, so that its average VSWR behaves well. Hence, antennas within their designed frequency bands may be used as a reference. The gain characteristic of this antenna is unimportant.

After a reverberating chamber is designed and its basic characteristics determined as outlined in this section, the radiated susceptibility measurements can be performed by placing the EUT at the test zone, routing its control cables to monitors outside the chamber, and preventing leakage to the exterior environment by using proper filtering processes,

needed. A test field has, of course, to be generated first by supplying power to the transmitting antenna. The desired field level may be established, as required, by gradually increasing the input power. The EUT's operation is monitored for malfunction while the tuner/stirrer is rotated through a complete revolution. The rotating rate should be low enough to allow sufficient time for the EUT to respond to the change in test field level. If a malfunction of EUT is observed for a particular tuner/stirrer position, the tuner/stirrer should be stopped and the net power to the transmitting antenna should be reduced until the malfunction ceases. The test results are then recorded and the test proceeds to the next frequency, etc., until the test is completed.

Radiated emission measurements are performed in a fashion reciprocal to susceptibility measurement or by using a substitution technique. In this case, the transmitting antenna is removed from the chamber because the EUT itself is the radiator. The power received by the reference antenna may be measured and used to determine the total power radiated by the EUT with the aid of the chamber quality factor (27), or the equivalent radiated far field by (28). Alternatively, the power radiated by the EUT may also be determined by measuring the equivalent power applied to a transmitting antenna substituting for the EUT, provided, of course, the same power is received by the reference antenna.

V. Microwave Anechoic Chambers

Microwave anechoic chambers are frequently used for a great variety of indoor EMC/EMI measurements and antenna calibrations. The NBS chamber is shown in Fig. 26.

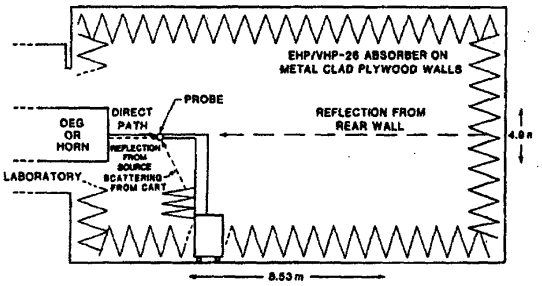

Fig. 26. A side view of the NBS anechoic room. The outside width is 6.7 m.

Rectangular pyramidal horns are used as sources of chamber illumination for frequencies above 500 MHz, and open-end waveguides (OEG) antennas are used below 500 MHz. The source antenna is positioned at the access doorway with its aperture in the plane of the absorber points on the chamber wall. A probe or other receiving antenna is carried by a cart mounted on precision tracks under the measurement axis, which can be moved 5 m longitudinally by a stepping-motor-drive system. The gaps in the absorber to accommodate each rail are 20 cm wide. This particular chamber was designed mainly to generate standard fields at 1- to 5-m separation distances for test antenna apertures less than $\lambda/2$ in diameter, for the purpose of calibrating radiation-hazard meters in the frequency range of 200 MHz to 40 GHz.

The prime requirement for an anechoic chamber in general is that a plane-wave field be produced to simulate a free-space environment over a test volume (inside the chamber) of dimensions sufficient to perform the test. This volume is frequently referred to as a quiet zone. For measurements involving high-gain antennas, this reflection-free quiet zone may be many wavelengths in diameter. The reflectivity level in the test zone serves as a measure of the chamber quality. This reflectivity level can be checked by measuring the relative insertion loss versus separation distance between a source antenna and a probe [10]. If the anechoic chamber is a perfect free-space simulator, the relative insertion loss varies with distance according to the free-space transmission formula [62]

$$P_r/P_t = G_s G_p(\lambda/4\pi d)^2 \tag{29}$$

where P_t is the net power transmitted by the source antenna in watts, P_r is the power received by the probe in watts, G_s and G_p are, respectively, the near-zone gains of the source and probe antennas, d is the antenna separation distance in meters, and λ is the wavelength in meters. Notice that the near-zone gains are involved because the source antenna and probe are, for the NBS chamber, placed within the near zones of each other. [On the other hand, if the probe is separated by a far-zone distance from the source antenna, G_s and G_p in (29) are just the ordinary antenna gains.]

The quality of the NBS chamber is evaluated by comparing the measured relative insertion loss and computed transmission loss over the 5-m distance. The relative losses rather than the absolute losses are compared because it is rather difficult to measure the gain product G_sG_p with more accuracy than the reflection error in the chamber. For measuring relative insertion losses, the probe (short dipole) gains are assumed to be constant with separation distance. This assumption is justified by the fact that the probe aperture dimension is much less than $\lambda/2$ and the near-zone/far-zone boundary is on the order of $\lambda/(2\pi)$. The gain of pyramidal horns is, however, calculated using the finite-range equations [63]. Based on Schelkunoff's derivation for the near-zone gain of a pyramidal horn, an improved expression which includes the reflected and diffracted fields from the horn interior and double diffraction at the aperture may also be used [64].

For the OEG antennas, mathematical formulas by modifying the Stratton–Chu formula [65] are available for calculating accurately the far-zone electric- and magnetic-plane radiated fields. The forward near-zone power patterns can be determined from these far-zone fields by use of the plane-wave scattering-matrix approach [66]. The integral of this near-zone power pattern then yields the near-zone gain [67], [68].

In the above calculations, it is assumed that the input impedance of the source and probe antennas and the power transmitted by the source antenna all remain constant. Typical results are presented in Figs. 27 and 28. Fig. 27 gives data for 200 MHz with an OEG (WR 3600) as the source antenna, and Fig. 28 shows data for 517 MHz with a horn antenna (SA 12-0.5) as the source. Clearly, the experimental results show excellent agreement with the calculated ones. The deviation between the two for low frequencies such as that displayed in Fig. 27 for 200 MHz is believed due to reflections or scattering from the cart,

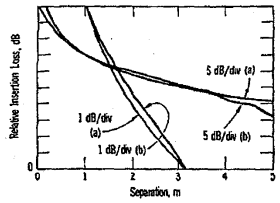

Fig. 27. Measured relative insertion loss between source and probe antennas (*b*) versus separation distance with free-space transmission loss curve (*a*) fitted at 1 m; frequency = 200 MHz; OEG as source antenna.

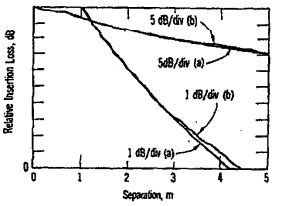

Fig. 28. Measured relative insertion loss between source and probe antennas (*b*) versus separation distance with free-space transmission-loss curve (*a*) fitted at 1 m; frequency = 517 MHz; horn antenna as source.

which is estimated to range from 0.5 dB at 200 MHz to 0 dB above 400 MHz, for a 1-m separation distance. Information on the VSWR of the chamber can also be extracted from this relative insertion-loss plot. Rear-wall reflections and source-to-probe interactions are often resolvable, but reflections from the ceiling, sidewalls, and floor are difficult to identify at frequencies below 500 MHz because the VSWR period is too long.

Additional potential error of the standard field generated in the test volume arises from the uncertainty in net power delivered to the source antenna. To compute more accurately this net power, we currently use the measuring system shown in Fig. 29, enabling us to measure the incident

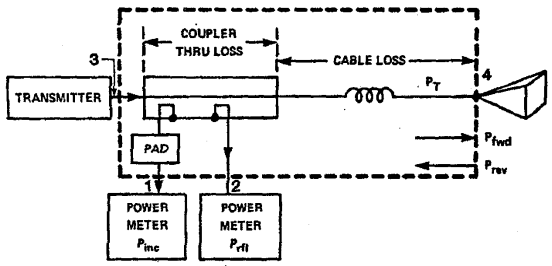

Fig. 29. Measuring the net power to a standard antenna.

and reflected powers with a dual directional coupler. The port terminations and numbering in Fig. 29 are as follows:

1. power meter to monitor forward power
2. power meter to monitor power reflected from the standard transmitting antenna
3. RF CW generation
4. standard transmitting antenna.

The net power delivered to a standard transmitting antenna is the difference between incident and reflected powers [69]

$$P_{net} = P_{inc} - P_{refl} = \frac{P_1}{1-|\Gamma_1|^2}\cdot\left|\frac{S_{34}}{S_{13}}\right|^2\cdot|g(S,\Gamma)|^2 - \frac{P_2}{1-|\Gamma_2|^2}\cdot\frac{1}{|S_{24}|^2}|h(S,\Gamma)|^2 \quad (30)$$

where P_1 and P_2 are, respectively, power meter readings at ports 1 and 2, Γ_1 and Γ_2 represent the corresponding reflection coefficients observed looking into power meters 1 and 2, S_{ij} is the scattering parameter defined as the ratio of the complex wave amplitude emerging from port i to that incident on port j, and $g(S,\Gamma)$ and $h(S,\Gamma)$ are functions of the system S-parameters and the reflection coefficients of ports 1, 2, and 4 [69].

For an ideal coupler, i.e., zero reflection coefficients for all coupler input ports and infinite directivity ($S_{11} = S_{22} = S_{33} = S_{44} = S_{14} = S_{41} = S_{23} = S_{32} = 0$), and for a matched power meter 1 ($\Gamma_1 = 0$), it can be shown [69] that $g(S,\Gamma) = h(S,\Gamma) = 1$. Unless the phases of the system S-parameters and the reflection coefficients are well determined, $g(S,\Gamma)$ and $h(S,\Gamma)$ are not calculable. The extent of deviation from unity is, therefore, taken to be an error contribution.

From (30), we see that the terms S_{34}/S_{13} and $1/S_{24}$ need to be measured in order to determine the net power. Although we could measure the magnitudes of S_{13}, S_{24}, and S_{34} with a network analyzer, the system developed here for establishing standard fields is a self-calibrating system, which utilizes a standard short circuit and a matched termination. When a short is placed at port 4 ($\Gamma_4 = 1$), the ratio of power measurements P_2 and P_1 gives

$$\frac{P_2}{P_1} = \left|\frac{S_{24}S_{34}}{S_{13}}\right|^2\frac{1-|\Gamma_2|^2}{1-|\Gamma_1|^2}(1+\Delta_1) \quad (31)$$

where Δ_1 is a small quantity much less than one, caused by directional coupler imperfections. Thus the term Δ_1 and uncertainty in the power ratio measurement P_2/P_1 make up the uncertainty in determining $|S_{24}S_{34}/S_{13}|^2$. The next step is to replace port 4 with a well-matched power meter and measure P_4 and P_1. The ratio gives

$$\frac{P_1}{P_4} = \left|\frac{S_{13}}{S_{34}}\right|^2\frac{1-|\Gamma_1|^2}{1-|\Gamma_4|^2}(1+\Delta_2). \quad (32)$$

Again, the small error Δ_2 and uncertainty in the power ratio measurement P_1/P_4 constitute the uncertainty in $|S_{13}/S_{34}|^2$. From (31) and (32), values for $|1/S_{24}|^2$ and $|S_{13}/S_{34}|^2$ are obtained. These may then be substituted into (30) to compute the net power. Thus an accurate calculation of the net power delivered to the source antenna and its near-zone gain more precisely determine the relative insertion loss of the anechoic chamber.

The major disadvantage associated with an anechoic chamber is its construction cost. Recent studies have led to the conclusion that an opportunity exists to extend the low-frequency range limit for anechoic-type chambers. Such chambers would be constructed using techniques similar to those for anechoic rooms—that is, they would be shielded and lined with absorbers. However, in order to achieve economy in size and cost, such chambers would no longer

be truly anechoic, and have been designated as absorber-lined chambers (ALC). The utilization of ALC for evaluating electromagnetic susceptibility has been discussed [70].

VI. Developments of Electric- and Magnetic-Field Probe

In order to measure quantitatively the EM environment, a small antenna, or probe, with an RF detector is often used. After sensing the RF field, the probe produces a dc voltage output which can be processed through the associated instrumentation to indicate the field level. Currently, there are two kinds of probes available, one sensing the electric-field strength and the other the magnetic-field strength.

Two types of instrumentation are normally used in a receiving system: one is the conventional field-strength meter consisting of a tunable meter or spectrum analyzer and a single antenna, which must be oriented for the desired field polarization. This kind of receiver generally offers high sensitivity and selectivity, and is not designed as a portable instrument for making quick surveys of the EM environment. The receiver thus acts as a frequency-selective voltmeter. The required conversion factor between the antenna pickup voltage (volts) and the electric-field strength (volts per meter) is the antenna factor. It must be determined experimentally for each antenna used in the system, at each frequency and orientation by calibrating the antenna in a known standard field.

The other type of instrumentation employs a nontunable sensor characterized by lower sensitivity but broad-band response. The antenna involved in this latter type preferably has a flat response over a wide frequency range and a nondirective pattern. It is generally designed for measuring relatively high-level fields exceeding 1 V/m, such as the region close to a transmitting antenna. The frequency of interest is generally above 300 kHz. Thus it can conveniently be used to assess a microwave hazard environment.

Earlier Models

The program carried out at NBS in the past was to develop various probes in the frequency range of 100 kHz to 18 GHz for measuring electric-field intensities of at least 0.1 V/m, or measuring magnetic-field intensities of 0.25 mA/m or more. The design principle of early probes was primarily based on temperature rise due to the absorption of RF energy [71]. Field strength was indicated either by the changing color of a liquid-crystal material, the change of resistance in a lossy dielectric, or by a glowing neon gas inside a miniature glass bulb located at the center of the sensor. Other types of probes developed at NBS include center-loading a short dipole with a miniature incandescent bulb about 2 mm long or a thermocouple heater [72]. The current induced in the bulb or heater by the field was then used as a measure of the field strength. All of these early models lacked adequate sensitivity, quick reaction time, good stability for calibration over a long period of time, dependable corrections for variations in ambient temperature, and thus satisfactory measurement repeatability.

Another early probe developed at NBS was an "active" antenna system consisting of three orthogonal dipoles, each sensing one component of the field (x, y, or z) [73]. This arrangement avoids requiring physical rotation of the probe. Because the dipoles are perpendicular to each other, the mutual-coupling effect is relatively insignificant. This system was designed for the frequency range of 15 kHz to 150 MHz. The dipoles, all electrically short over the entire frequency range, are connected to a conventional tunable RF receiver by a fiber-optic link. The antenna pickup is amplified first and then applied as modulation to the infrared (IR) output of a high-speed light-emitting diode (LED). The system is considered active in the sense that the RF signal is amplified before detection or modulation process. The modulated IR signals are guided through glass fibers to avalanche photodiodes in the metering unit. These glass lines provide essentially perfect electrical isolation between the sensing antennas and metering unit. Photodetectors recover the total RF modulation from the IR carrier for input to the RF receiver. The readout indication at each frequency is proportional to a single component of the probed electric field. A root-sum-square (rss) circuit is also incorporated in the system to give the total magnitude of the three field components.

The most important advantage of this probe is that complete signal information can be recovered, including not only the signal strength but also frequency and phase characteristics. The sensitivity of this system is also adequate. It may be noted that the probe sensitivity decreases rapidly above the designed upper frequency limit of 150 MHz with no unwanted enhancement at the dipole self-resonant frequency. One of the disadvantages is the rather low dynamic range. In fact, both the tangential sensitivity and linear dynamic range depend on the tuned frequency, noise figure, and bandwidth of the auxiliary receiver included in the system. Another disadvantage is the limited upper frequency caused by the limitation of LED speed. [However, heterodyne conversion employing an RF local oscillator inside the active dipole could be used to achieve higher effective signal frequency, but this approach has not been pursued.] In addition, the switching speed between measurements of the three field components is relatively slow because only one RF receiver was used for all three dipoles. The level of spurious responses and intermodulation distortion is also rather high.

Recent Models

One of the recent probes developed at NBS is the broad-band, isotropic, real-time, electric-field sensor (BIRES) [74], [75]. This probe covers a much broader frequency band, typically from 10 MHz to 1 GHz, also using three orthogonal dipoles. Each dipole is fabricated by depositing a thin film of metal alloy with varying resistivity on a glass rod. The alloy, which consists of approximately 70 percent nickel, 15 percent chromium, 10 percent iron, 2 percent titanium, and others, has a high resistivity and low temperature coefficient. The glass rod, 15 cm long and 0.7 cm in diameter, serves as a substrate for the deposited film. The antenna becomes a half-wave dipole at approximately 1 GHz. The required resistive loading is about 5 kΩ/m at the center of each dipole, 10 kΩ/m at midpoint between the center and ends, and infinite at the ends of the dipole. It is possible to calculate the required thin-film thickness. Typically, this is about 240 nm at the center, 100 nm at the midpoint, and zero at the ends.

Because the tapered resistive loading makes the internal impedance per unit length a proper function of position

along the dipole, the resulting current distribution on the antenna is a pure outward-traveling wave. Hence the probe has linear amplitude and phase responses over a broad frequency band, and as such may be used to measure fast time-varying signals with minimum pulse-shape distortion. The probe also has a filtering action so that EM signals outside the designed frequency range will be rejected, preventing out-of-band responses. In addition to amplitude, phase, and frequency, the probe also provides polarization information of the EM environment.

The BIRES probe uses metal coax cables to convey RF signals from the antenna to the metering unit. Thus the electrical isolation of the antenna and resulting isotropy is not as good as the other probes discussed previously. Because the RF signal voltage delivered to the conventional 50-Ω receiver from the dipoles is not independent of signal frequency, an RF shaping amplifier is incorporated in the system for frequency compensation. The tangential sensitivity and linear dynamic range also depend on the signal frequency and bandwidth of the auxiliary receiver used.

Quite often, the regions being measured are close to radiating sources. In such cases, the field structure is very complicated, including reactive (stored) and real (propagated) components, standing waves, unknown phases, and unclear field polarization. The most practical manner of surveying this kind of field environment is to use isotropic RF probes, independent of orientation and the direction of wave propagation, as hazard meters. It is important that the probe be small in size and thus be able to resolve the spatial variations in field strength. Furthermore, the field being surveyed should not be perturbed substantially by the operator or equipment associated with the measurement. The end result of meeting these requirements is represented by the NBS' development of an "isolated" probe system [76]. A typical response at 20 dBV/m (10 V/m) of the NBS isotropic electric-field monitor (EFM-5) is shown in Fig. 30. A family of NBS designed electric-field strength meters using isolated probes has been adopted as commercial meters by private industry.

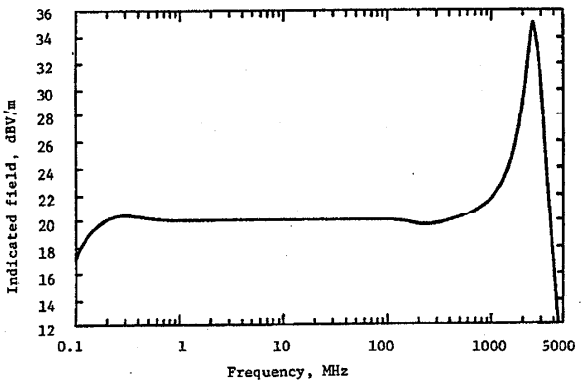

Fig. 30. Typical response of the NBS isotropic electric-field monitor (EFM-5).

The probe consists of three short dipoles mounted orthogonally in three notches cut near the end of a plastic tube. The dipoles are then embedded in a foam sphere 10 cm in diameter. The difference in transmission line between this probe and the BIRES discussed earlier is that this probe unit employs three high-resistance plastic twinleads inside the dielectric handle to bring the dc voltage to the receiver. These lines also act as *RC* low-pass filters for the demodulated signal coming from the dipole. Nonlinear circuitry included in the metering unit can be used to give the rss value of the three perpendicular field components at the measuring point, to represent the total effect of all electric field components, all polarizations, all arrival directions, and all frequencies within the passband of the antenna/filter combination. The unit also includes switches to permit measurement of a single field component only, allowing a choice of measuring either the average or peak amplitude of modulated signals. Typical applications for this probe system are 1) measurement of possible RF hazards caused by diathermy equipment, industrial RF heaters, plastic sealers, and near fields of transmitting antennas; 2) survey of ambient fields for low-level RF pollution caused by AM, FM, TV, CB, and other broadcasting services; 3) check of EM fields in sensitive areas containing electroexplosive devices or flammable fluids; and 4) check of field strength in sites having instruments which may be degraded by the presence of RF radiation.

Although the isolated probe has a fairly flat response over the designed frequency range of 0.2 MHz to 1 GHz, it is found that it also responds to high frequencies. Therefore, RF fields due to harmonics and other frequencies all contribute to the meter indication. Also, the measurement accuracy is normally reduced for pulsed fields that have pulsewidths lower than 0.3 ms, because of the limited charging time of the *RC* filter line included in the system. In addition, a possible erroneous increase in meter indication occurs when measuring multifrequency fields.

Another isotropic probe (MFM-10) for measuring primarily magnetic-field intensities was developed, based on the same principle and incorporates much of the instrumentation used for the isolated electric-field probe described above [77]. Three small orthogonal loops were used instead of short dipoles. It provides near-zone measurement of magnetic fields over a dynamic range of 0.1 to 12 A/m with a relatively flat response in the frequency range of 300 kHz to 100 MHz. It also is capable of measuring each of the three orthogonal field components in addition to the total field magnitude.

The mechanical and electrical configurations of an individual loop in this probe are illustrated in Fig. 31. The internal portion of each loop is composed of 5 turns of wire with a detector at the loop center and a filter capacitor C_3 connected between the two ends. The diode, D_1, provides rectification of the RF signal induced in the loop. The diode shunting elements, R_1 and C_1, help produce a flat frequency response. The values of R_1, C_1, and C_3 are critical to the proper shaping of this response. A normalized response curve given in Fig. 32 shows that the maximum variation with frequency is less than ± 1 dB.

Two subsystems have been developed to be used with any of the broad-band isotropic probes. One of them uses the fast Fourier transform (FFT) technique [78]. During each measurement, the total amplitude of antenna pickups over a given frequency band is recorded on a high-speed tape recorder in the time domain. These recordings are later analyzed with a computer by FFT processing to obtain a three-dimensional display of field strength versus frequency,

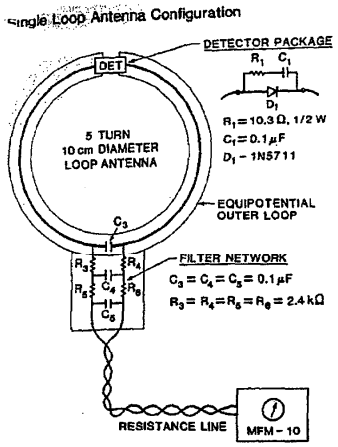

Fig. 31. NBS magnetic-field meter (MFM-10).

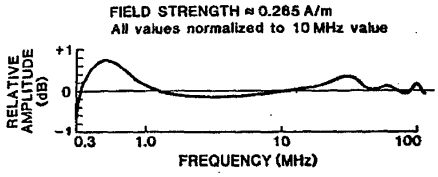

Fig. 32. Normalized response curve of MFM-10.

with time as a third parameter. This device, therefore, enables an analysis of changes of the spectrum occupancy with time. Another subsystem provides a microprocessor control for rapid data acquisition of three orthogonal field components and the total field amplitude [79], [80]. Both of these approaches require previous calibration of the antenna factors involved.

Future Models

A shortcoming of most isotropic broad-band probes is the relatively long response time of the RF sensor. It would be impossible or difficult to measure directly the peak-to-average ratio of a modulated field or the momentary maximum envelope intensity in the beam center of a scanning antenna. It is often advantageous or desirable to have the capability for observing the modulation on a signal being measured. In addition, the biological importance of measuring peak levels of RF pulses has not been established partly because the measuring instrumentation is not yet commercially available. To make up for this shortcoming, a new system employing laser diodes, single-mode fiber-optic guides, and optical modulators to replace the conventional coax cables in any of the isotropic broad-band probes is being developed. Initial results are very promising. This approach could result in an EMI measuring antenna with a short response time, much broader bandwidth, and good sensitivity.

To date all the practical field strength meters measure either the electric field or magnetic field separately. A new probe is being developed at NBS to measure the electric and magnetic fields simultaneously so that an EM environment may be characterized more completely [81]. This type of probe is particularly needed for measuring the near field where the magnitude and phase angle of the wave impedance are unknown, and the electric- and magnetic-field vectors are not necessarily orthogonal to each other nor in the same time phase. Thus the new device is intended to measure not only the polarization ellipse of the field vectors in a near-field environment, but also the time-dependent Poynting vector to indicate the energy flow. The probe consists of three electrically isolated doubly loaded loops with the capability of measuring the sum and difference of the detected voltages at the two opposite ends of each loop. A diagram of a single loop with equal loads of Z_L is shown in Fig. 33. Currents developed in the loads correspond to the electric-dipole and magnetic-loop responses. More precisely, across one load, the electric response adds to the magnetic response, while across the other load, the electric response subtracts from the magnetic response. To separate the currents, a 0°/180° hybrid is used to obtain the sum and difference of the currents. Thus the sum current I_Σ gives a measure of the magnetic field, whereas the difference current I_Δ gives a measure of the electric field.

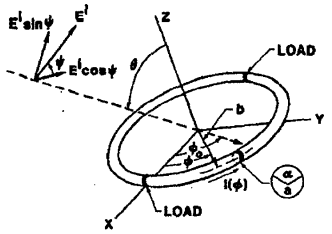

Fig. 33. A single loop with equal loads in a new probe for measuring simultaneously the electric and magnetic fields.

The calculated sum and difference currents in a loop with a load impedance of 200 Ω are presented in Fig. 34. The real part of the currents increases with frequency up to about 200 MHz. The magnetic-loop current is larger than the electric-dipole current up to 100 MHz, while the electric-dipole current becomes more dominant above 100 MHz.

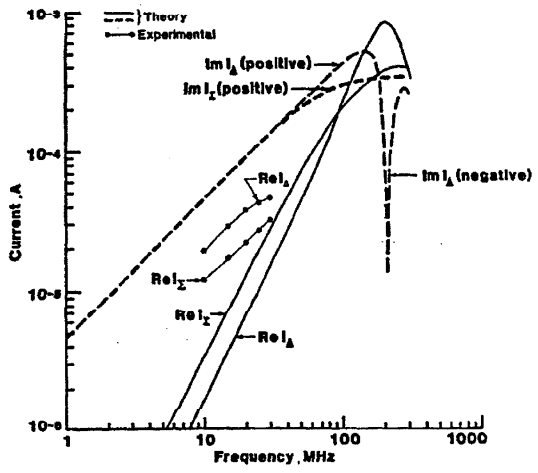

Fig. 34. Magnetic-loop (I_Σ) and electric-dipole (I_Δ) currents of a loop antenna with Z_L = 200 Ω.

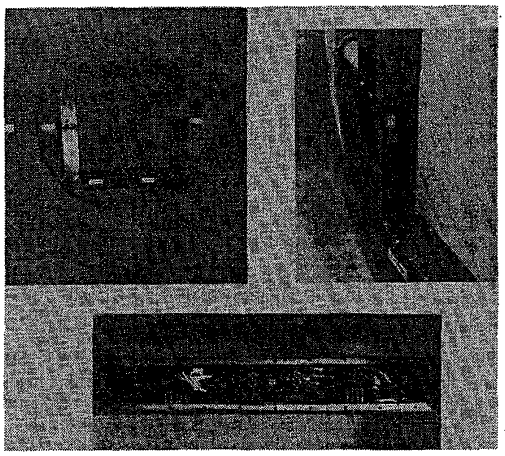

Fig. 35. An experimental loop model for measuring simultaneously the electric and magnetic fields.

An experimental loop model with a radius of 0.16 m and wire radius of 0.02 m is shown in Fig. 35. This loop is doubly loaded with 200 Ω by using 4:1 baluns and 50-Ω resistive loads. Zero-bias Schottky diodes are used as detectors, with high-resistance plastic transmission lines connecting the loop and high-impedance dc voltmeter. Measured values of the real part of I_Σ and I_Δ for this loop placed in a TEM cell with a known incident electric field of 1 V/m are included in Fig. 34. Although there is some discrepancy between the theoretical and experimental results, which may be associated with the balun impedance, the preliminary results indicate the validity of the theory.

Fig. 36 shows the real parts of the magnetic-loop and electric-dipole currents as a function of load impedance at 10 MHz. It reveals that there is a critical load impedance, for example 260 Ω at 10 MHz, for which the two currents are equal. Below this critical impedance, the magnetic-loop current is greater than the electric-dipole current. Above this impedance, the reverse is true. Critical load impedance has only a slight frequency dependence, ranging from 200 to 260 Ω for the frequency range of 1 to 100 MHz [81].

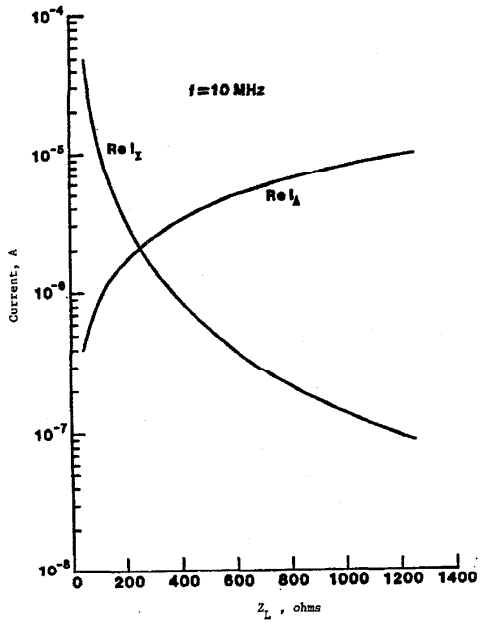

Fig. 36. Real parts of magnetic-loop and electric-dipole currents of a loop antenna as a function of load impedance at 10 MHz.

Diode Model

Some of the probes described earlier use a diode to convert the electric field being surveyed to a dc voltage. The main advantage of including a diode is to make the frequency response of the probe very flat, so the system can be used as a portable and compact hazard meter. Otherwise, since the input impedance of a probe (short dipole) without a diode is mostly capacitive, the antenna factor for such a probe is, in accordance with (1), frequency sensitive. It would be difficult to determine the unknown field strength without also detecting the frequency by a spectrum analyzer.

A beam-lead Schottky-barrier diode is usually chosen for this purpose. It has good high-frequency performance due to a small junction capacitance, high sensitivity, and low-noise characteristics. When an electrically short dipole is terminated with such a diode, the effect of loading may be analyzed by the simple Thévenin's equivalent circuit shown in Fig. 37, where the induced open-circuit voltage $V_i(t)$ at

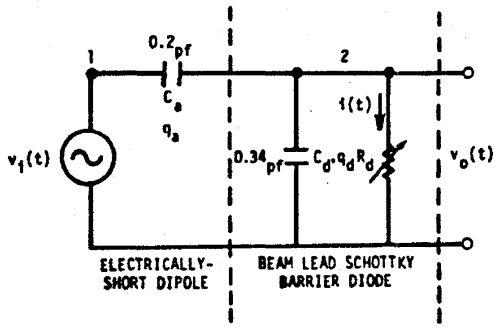

Fig. 37. Thévenin's equivalent circuit of a probe–diode system.

the diode terminal is given by

$$V_i(t) = E_{\text{inc}}(t)\,\ell_e \tag{33}$$

with E_{inc} as the tangential incident electric field, and ℓ_e the effective length of the dipole. The element C_a in Fig. 37 is the equivalent driving-point capacitance of the short dipole, and the parallel combination of capacitance C_d and nonlinear resistance R_d represents a simplified model of the diode.

For an electrically short dipole, the effective length and the driving-point capacitance are given respectively by [82]

$$\ell_e = \frac{h(\Omega - 1)}{\Omega - 2 + \ln 4} \quad \text{m} \tag{34}$$

and

$$C_a = \frac{2\pi\epsilon_0 h}{\Omega - 2 + \ln 4} \quad \text{F} \tag{35}$$

where h is the half physical length of a dipole in meters, ϵ_0 is the free-space permittivity in farads per meter, Ω is the

antenna thickness factor defined by $\Omega = 2\ln(2h/a)$, and a is the dipole radius in meters. For example, when $h = 0.02$ m, $a = 2.84(10)^{-5}$ m, we have $\Omega = 14.50$, $\ell_e = 1.94(10)^{-2}$ m, and $C_a = 0.10$ pF. Note that the symbol Ω should not be confused with the unit for a resistance.

The current flowing through the nonlinear resistance R_d of the diode may be characterized by its v–i relationship

$$i(t) = I_s(e^{\alpha V_0(t)} - 1) \tag{36}$$

where I_s is the saturation current, which is assumed in this case to be $2(10)^{-9}$ A, $V_0(t)$ is the voltage in volts across the diode junction, $\alpha = q/nKT = 38\ V^{-1}$, q is the electron charge [$1.6(10)^{-19}$ C], n is the diode ideality factor [~ 1.05], K is the Boltzmann's constant [$1.38(10)^{-23}$ J/K], and T is the absolute room temperature [~ 290 K].

At frequencies approximately higher than 10 MHz, we obtain the detected dc voltage averaged over complete cycle as [83]

$$V_0 = -\frac{\alpha}{4}\left[\frac{V_i}{1 + C_d/C_a}\right]^2 = -\frac{\alpha \ell_e^2 E_{inc}^2}{4(1 + C_d/C_a)^2} \tag{37}$$

for a small sinusoidal induced steady-state voltage V_i [$\leqslant 1$ V]; and

$$V_0 = -\frac{V_i}{1 + C_d/C_a} = -\frac{\ell_e E_{inc}}{1 + C_d/C_a} \tag{38}$$

for a relatively strong V_i [> 1 V].

Thus V_0 is a square-law function of the incident electric field E_{inc} when $V_i \leqslant 1$ V, and is a linear function of E_{inc} when $V_i > 1$ V.

The frequency response of V_0 with $E_{inc} = 1$ V/m for a sample probe and diode system is shown in Fig. 38, where the analytical solutions are obtained by solving a first-order nonlinear differential equation in accordance with the equivalent circuit shown in Fig. 37, while the numerical solutions are achieved by using an approximate time-stepping difference equation [83]. From Fig. 38, we see that the frequency response is indeed very flat. The inverse of these curves represents the antenna factor for the entire system.

VII. Concluding Remarks and Discussions

We have reviewed some EMC/EMI measurement methodologies, which are of industrial interest. In particular, measurements using the facilities such as open sites, TEM cells, reverberating chambers, and anechoic rooms have been addressed. Advantages and limitations for each of these facilities, technical justifications, and considerations for interpreting the measurement results have been discussed. A related topic of probes including modeling of diodes which are parts of the probe system has also been presented in order to determine the overall antenna factor.

To maintain adequate electric isolation but to reduce strong signal reflections as those associated with the conventional shielded rooms, buried or underground low-Q enclosures may be used as an alternate means for performing EMC/EMI tests. Existing or natural underground caves, mine tunnels of sufficient depth below the earth surface, or fabricated buried rooms with a limited overburden constructed from layered soil materials may belong to this category.

One topic of future importance but exceeding the scope of this paper is the measurement involving whole systems of large objects. If every component of the system were independently powered and operated, the system overall EMC/EMI characteristics, whether considered from emission or susceptibility points of view, would probably not be changed. However, wiring harnesses, component metallic structures, and interconnecting cables tie all components together to form a very interactive system, which couples energy at its own natural resonant frequencies. Whole-system testings are then necessary to evaluate the system response to determine whether the various components can function properly in the system environment. New facilities allowing such a testing and interpretation of the measurement results will be a challenge for future activities.

Theoretical and practical studies concerning EMC/EMI measurements of broad-band pulsed signals are another important area needed to be addressed, since some electronic devices and systems are more susceptible to short-duration impulse interference than CW interference.

A third important area relating to EMC/EMI studies is the methods involved in processing the measurement data. In general, because of the complexity of EM fields, no meaningful conclusion may be drawn based on a single test result. Simple average technique or more sophisticated statistical means such as two-sample variance analysis, amplitude probability distribution (which is commonly used for analyzing the performance of communication systems), average cross rate, interpulse spacing, and pulse duration distributions for the impulsive EMI, depending on the actual situation at hand, may be used for data-processing purpose [84].

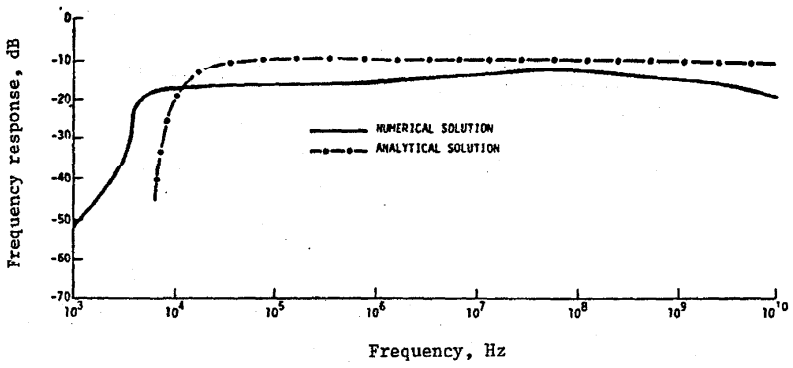

Fig. 38. Frequency response of a typical probe–diode system with $E_{inc} = 1$ V/m.

ACKNOWLEDGMENT

The authors are grateful to acknowledge the contributions received from many individuals of the Electromagnetic Fields Division, NBS, Boulder, CO: P. F. Wilson and D. A. Hill for their critical review of the manuscript and constructive suggestions for improvement; J. P. Randa for his useful comments; and C. K. S. Miller, H. E. Taggart, F. X. Ries, and J. W. Adams for their participation in discussions during the organization of this paper.

REFERENCES

[1] *IEEE Standard Dictionary of Electrical and Electronics Terms*, ANS/IEEE Std 100-1977, 2nd ed., F. Jay, Ed. New York: Wiley, 1977.

[2] E. E. Donaldson, W. R. Free, D. W. Robertson, and J. A. Woody, "Field measurements made in an enclosure," *Proc. IEEE*, vol. 66, no. 4, pp. 464–472, Apr. 1978.

[3] Jan-I-225, Joint Army-Navy Specification, "Interference measurements, radio methods of, 150 kilocycles to 20 Megacycles (for components and complete assemblies)," June 14, 1945.

[4] MIL-STD-462, "Electromagnetic interference characteristics, measurement of," July 31, 1967.

[5] "FCC methods of measurement of radio emission from computing devices," FCC Rules, pt. 15, Subpt. J, Appendix A (July, 1981) and FCC 83-352 order on general docket 80-284, Appendix B, July, 1983.

[6] C. R. Burrows, "Radio propagation over plane earth-field strength curves," *Bell Syst. Tech. J.*, vol. 12, pp. 45–75, Jan. 1937.

[7] "Recommended methods of measurement of radiated and conducted interference from receivers for amplitude-modulation, frequency-modulation, and television broadcast transmission," Int. Electro-Tech. Commission Pub. 106, 1974.

[8] "Calibration of a radiation measurement site- site attenuation," FCC docket 21371, Appendix A, Bulletin OCE 44, Sept. 1977.

[9] T. Kawana and S. Miyajima, "Theoretical investigation of site attenuation by means of mutual impedance between antennas," in *Proc. 3rd Symp. Tech. Exhibition on EMC* (Rotterdam, The Netherlands), pp. 83–88, 1979.

[10] R. G. FitzGerrell, "Using free-space transmission loss for evaluating anechoic chamber performance," *IEEE Trans. Electromag. Compat.*, vol. EMC-24, no. 3, pp. 356–358, Aug., 1982.

[11] International Electro-Technical Commission Document 12A (Secretariat), Apr. 1978.

[12] International Special Committee on Radio Interference (ISCRI) Pub. 13, 1975.

[13] R. G. FitzGerrell, "E-fields over ground," presented at the IEEE Int. Symp. on EMC, Arlington, VA, 1983.

[14] A. A. Smith, Jr., R. F. German, and J. B. Pate, "Calculation of site attenuation from antenna factors," *IEEE Trans. Electromag. Compat.*, vol. EMC-24, no. 3, pp. 301–316, Aug., 1982.

[15] E. C. Jordan, *Electromagnetic Waves and Radiating Systems*. Englewood Cliffs, NJ: Prentice-Hall, 1950.

[16] C. O. Stearns, "Mutual impedances between parallel, side-by-side, infinitesimally thin half-wave dipoles," NBS Rep. 6798, Sept. 1961.

[17] K. A. Norton, "The propagation of radio waves over the surface of the earth and in the upper atmosphere, pt. I," *Proc. IRE*, vol. 24, no. 10, pp. 1367–1387, Oct. 1936.

[18] ———, "The propagation of radio waves over the surface of the earth and in the upper atmosphere, pt. II," *Proc. IRE*, vol. 25, no. 9, pp. 1203–1236, Sept. 1937.

[19] K. Fukuzawa, M. Tada, T. Yoshikawa, K. Ouchi, and R. Sato, "A new method of calculating 3-meter site attenuation," *IEEE Trans. Electromag. Compat.*, vol. EMC-24, no. 4, pp. 389–397, Nov. 1982.

[20] R. F. Harrington, *Field Computation by Moment Methods*. New York: Macmillan, 1968.

[21] W. S. Bennett, "Comment on Calculation of site attenuation from antenna factors," *IEEE Trans. Electromag. Compat.*, vol. EMC-25, no. 2, p. 121, May 1983.

[22] F. M. Greene and M. Solow, "Development of very-high-frequency field-intensity standards," *J. Res. Nat. Bur. Stand.*, vol. 44, pp. 527–547, May, 1950.

[23] H. E. Taggart and J. L. Workman, "Calibration principles and procedures for field strength meters (30 Hz to 1 GHz)," NBS Tech. Note 370, Mar. 1969.

[24] A. A. Smith, Jr., "Standard-site method for determining antenna factors," *IEEE Trans. Electromag. Compat.*, vol. EMC-24, no. 3, pp. 316–322, Aug. 1982.

[25] W. R. Free, "Radiated EMI measurements in shielded enclosures," in *Proc. IEEE Int. Symp. on EMC* (Washington, DC), p. 43, 1967.

[26] J. C. Tippet, "Modal characteristics of rectangular coaxial transmission line," PhD dissertation, Dept. of Electrical Engineering, Univ. of Colorado, Boulder, 1978.

[27] M. L. Crawford and J. L. Workman, "Asymmetric versus symmetric TEM cell for EMC measurements," presented at the IEEE Int. Symp. on EMC, Atlanta, GA, 1978.

[28] W. F. Decker, W. A. Wilson, and M. L. Crawford, "Construction of a large transverse electromagnetic cell," NBS Tech. Note 1011, Feb. 1979.

[29] M. L. Crawford, "Generation of standard EM fields using TEM transmission cells," *IEEE Trans. Electromag. Compat.*, vol. EMC-16, no. 4, pp. 189–195, Nov. 1974.

[30] J. C. Tippet, D. C. Chang, and M. L. Crawford, "An analysis and experimental determination of the cutoff frequencies of higher-order TE modes in a TEM cell," NBSIR 76-841, June, 1976.

[31] J. C. Tippet and D. C. Chang, "Higher order modes in rectangular coaxial line with infinitely thin inner conductor," NBSIR 78-873, Mar. 1978.

[32] ———, "Radiation characteristics of dipole sources located inside a rectangular, coaxial transmission line," NBSIR 75-829, Jan. 1976.

[33] R. Mittra and T. Itoh, "A new technique for the analysis of the dispersion characteristics of microstrip lines," *IEEE Trans. Microwave Theory Tech.*, vol. MTT-19, no. 1, pp. 47–56, Jan. 1971.

[34] L. Gruner, "High order modes in rectangular coaxial waveguides," *IEEE Trans. Microwave Theory Tech.*, vol. MTT 15, no. 8, pp. 483–485, Aug. 1967.

[35] M. L. Crawford, J. L. Workman, and C. L. Thomas, "Expanding the bandwidth of TEM cells for EMC measurements," *IEEE Trans. Electromag. Compat.*, vol. EMC-20, no. 3, pp. 368–375, Aug. 1978.

[36] D. A. Hill, "Bandwidth limitations of TEM cells due to resonances," *J. Microwave Power*, vol. 18, no. 2, pp. 181–195, 1983.

[37] M. L. Crawford, "Techniques for measurement of electromagnetic radiation and susceptibility of electronic equipment," in *1st Symp. Tech. Exhibition on EMC* (Montreux, Switzerland), pp. 38–44, 1975.

[38] M. L. Crawford and J. L. Workman, "Using a TEM cell for EMC measurements of electronic equipment," NBS Tech. Note 1013, Apr. 1979.

[39] I. Sreenivasiah, D. C. Chang, and M. T. Ma, "Characterization of electrically small radiating sources by tests inside a transmission line cell," NBS Tech. Note 1017, Feb. 1980.

[40] I. Sreenivasiah, D. C. Chang, and M. T. Ma, "Emission characteristics of electrically small radiating sources from tests inside a TEM cell," *IEEE Trans. Electromag. Compat.*, vol. EMC-23, no. 3, pp. 113–121, Aug. 1981.

[41] M. T. Ma and G. H. Koepke, "A method to quantify the radiation characteristics of an unknown interference source," NBS Tech. Note 1059, Oct. 1982.

[42] ———, "Uncertainties in extracting radiation parameters for an unknown interference source based on power and phase measurements," NBS Tech. Note 1064, June, 1983.

[43] G. H. Koepke and M. T. Ma, "A new method for determining the emission characteristics of an unknown interference source," presented at the 5th Symp. Tech. Exhibition on EMC, Zurich, Switzerland, 1983.

[44] M. L. Crawford and J. L. Workman, "Predicting free-space radiated emissions from electronic equipment using TEM cell and open-field site measurements," in *Proc. IEEE Int. Symp. on EMC* (Baltimore, MD), pp. 80–85, 1980.

[45] M. L. Crawford and C. L. Thomas, "Converting a rectangular shielded enclosure into a TEM transmission cell for EMI measurements," presented at the IEEE Int. Symp. on EMC, Seattle, WA, 1977.
[46] B. E. Roseberry and R. B. Schulz, "A parallel-strip line for testing RF susceptibility," *IEEE Trans. Electromag. Compat.*, vol. EMC-7, no. 2, pp. 142–150, June 1965.
[47] P. Groenveld and A. DeJong, "A simple RF immunity test set-up," presented at the 2nd Symp. Tech. Exhibition on EMC, Montreux, Switzerland, 1977.
[48] J. B. Pate and J. D. Williams, "The parallel plate chamber as a receiving instrument for measuring electrically small devices," presented at the IEEE Int. Symp. on EMC, Seattle, WA, 1977.
[49] G. Meyer, "The TEM measuring line—A critical overview," presented at the 4th Symp. Tech. Exhibition on EMC, Zurich, Switzerland, 1981.
[50] J. L. Bean and R. A. Hall, "Electromagnetic susceptibility measurements using a mode-stirred chamber," presented at the IEEE Int. Symp. on EMC, Atlanta, GA, 1978.
[51] P. Corona, "Electromagnetic reverberating enclosures: behavior and applications," *Alta Frequ.*, vol. 49, pp. 154–158, 1980.
[52] P. Corona, G. Latmiral, E. Paolini, and L. Piccioli, "Performance of a reverberating enclosure for power measurements in the microwave range," in *2nd Symp. Tech. Exhibition on EMC* (Montreux, Switzerland), pp. 419–423, 1977.
[53] P. Corona, A. DeBonitatibus, G. Ferrara, and E. Paolini, "Electromagnetic enclosures behavior—comparison data analysis," in *3rd Symp. Tech. Exhibition on EMC* (Zurich, Switzerland), pp. 231–236, 1979.
[54] P. Corona, G. Latmiral, and E. Paolini, "Performance and analysis of a reverberating enclosure with variable geometry," *IEEE Trans. Electromag. Compat.*, vol. EMC-22, no. 1, pp. 2–5, Feb. 1980.
[55] P. Corona, G. Latmiral, E. Paolini, and L. Piccioli, "Use of a reverberating enclosure for measurements of radiated power in the microwave range," *IEEE Trans. Electromag. Compat.*, vol. EMC-18, no. 2, pp. 54–59, May 1976.
[56] B. H. Liu, D. C. Chang, and M. T. Ma, "Eigenmodes and the composite quality factor of a reverberating chamber," NBS Tech. Note 1066, Aug. 1983.
[57] ____, "Design consideration of reverberating chambers for electromagnetic interference measurements," in *Proc. IEEE Int. Symp. on EMC* (Washington, DC), pp. 508–512, 1983.
[58] H. A. Mendes, "A new approach to electromagnetic field-strength measurements in shielded enclosures," in *Wescon Tech. Papers* (Los Angeles, CA, Aug. 20–23, 1968).
[59] R. F. Harrington, *Time-Harmonic Electromagnetic Fields*. New York: McGraw-Hill, 1961.
[60] J. M. Roe, "An improved technological basis for radiated susceptibility and emission specifications," presented at the IEEE Int. Symp. on EMC, Atlanta, Ga, 1978.
[61] M. L. Crawford, "Evaluation of a reverberating chamber facility for performing EM radiated field susceptibility measurements," NBSIR 81-1638, Feb. 1981.
[62] S. A. Schelkunoff, *Electromagnetic Waves*. New York: Van Nostrand Reinhold, 1943.
[63] E. V. Jull, "Finite-range gain of sectoral and pyramidal horns," *Electron. Lett.*, vol. 6, no. 21, pp. 680–681, Oct. 15, 1970.
[64] ____, "Errors in the predicted gain of pyramidal horns," *IEEE Trans. Antennas Propagat.*, vol. AP-21, no. 1, pp. 25–31, Jan. 1973.
[65] J. A. Stratton, *Electromagnetic Theory*. New York: McGraw-Hill, 1941.
[66] D. M. Kerns, *Plane-Wave Scattering-Matrix Theory of Antennas and Antenna–Antenna Interactions*, NBS Monograph 162, 1981.
[67] A. D. Yaghjian, "Approximate formulas for the far fields and gain of open-ended rectangular waveguide," NBSIR 83-1689, May 1983.
[68] ____, "Efficient computation of antenna coupling and fields within the near-field region," *IEEE Trans. Antennas Propagat.*, vol. Ap-30, no. 1, pp. 133–138, Jan. 1982.
[69] R. D. Orr and M. Kanda, "Evaluation of microwave anechoic chamber measurements," in preparation.
[70] T. Pavlasek, "The e.m. environment, its simulation and measurement," *Can. Elec. Engr. J.*, vol. 6, no. 2, pp. 3–8, 1981.
[71] R. R. Bowman, "Some recent developments in the characterization and measurement of hazardous electromagnetic fields," in *Proc. Int. Symp. on Biolog. Effects and Health Hazards of Microwave Rad.* (Warsaw, Poland), pp. 217–227, Oct. 1973.
[72] E. Aslan, "Electromagnetic radiation survey meter," *IEEE Trans. Instrum. Meas.*, vol. IM-19, pp. 368–372, Nov. 1970.
[73] E. B. Larsen, J. R. Andrews, and E. E. Baldwin, "Sensitive isotropic antenna with fiber-optic link to a conventional receiver," NBSIR 75-819, Sept. 1976.
[74] M. Kanda, "A relatively short cylindrical broadband antenna with tapered resistive loading for picosecond pulse measurements," *IEEE Trans. Antennas Propagat.*, vol. AP-26, pp. 439–447, May 1978.
[75] M. Kanda and F. X. Ries, "A broadband isotropic real-time electric-field sensor (BIRES) using resistively loaded dipoles," *IEEE Trans. Electromag. Compat.*, vol. EMC-23, pp. 122–132, Aug. 1981.
[76] E. B. Larsen and F. X. Ries, "Design and calibration of the NBS isotropic electric-field monitor (EFM-5), 0.2 to 1,000 MHz," NBS Tech. Note 1033, Mar. 1981.
[77] L. D. Driver and J. E. Cruz, "Development of the NBS isotropic magnetic-field meter (MFM-10, 300 kHz to 100 MHz," in *Proc. IEEE Int. Symp. on EMC* (Santa Clara, CA), pp. 460–467, Sept. 1982.
[78] W. D. Bensema, "A noise spectrum measurement system using the fast Fourier transform," *IEEE Trans. Electromag. Compat.*, vol. EMC-19, no. 2, pp. 37–43, May 1977.
[79] G. R. Reeve, "Synthesized isotropic pattern antennas for EM field measurements," in *Proc. IEEE Int. Symp. on EMC* (Boulder, CO), pp. 36–42, Aug. 1981.
[80] W. D. Bensema, "Broadband orthogonal array system microprocessor control and computation," in *Proc. IEEE Int. Symp. on EMC* (Boulder, CO), pp. 43–46, Aug. 1981.
[81] M. Kanda, "An electromagnetic near-field sensor for simultaneous electric and magnetic-field measurements," *IEEE Trans. Electromag. Compat.*, vol. EMC-26, pp. 102–110, Aug. 1984.
[82] R. W. P. King, *The Theory of Linear Antennas*. Cambridge, MA: Harvard Univ. Press, 1956, pp. 184 and 487.
[83] M. Kanda, "Analytical and numerical techniques for analyzing an electrically short dipole with a nonlinear load," *IEEE Trans. Antennas Propagat.*, vol. AP-28, no. 1, pp. 71–78, Jan. 1980.
[84] ____, "Time and amplitude statistics for electromagnetic noise in mines," *IEEE Trans. Electromag. Compat.*, vol. EMC-17, no. 3, pp. 122–129, Aug. 1975.